*Polymer Solutions: An Introduction to Physical Properties.* Iwao Teraoka

ISBNs: 0-471-38929-3 (Hardback); 0-471-22451-0 (Electronic)

# 4

# Thermodynamics and Dynamics of Semidilute Solutions

## 4.1 SEMIDILUTE POLYMER SOLUTIONS

So far we have paid attention mostly to dilute solutions, $c < c^*$, in which polymer chains are more or less separated from each other. Chapter 2 focused on thermodynamics, and Chapter 3 focused on dynamics. These solutions were mostly ideal. We also learned how the concentration $c$ might change the thermodynamics and dynamics, as represented by the osmotic pressure and the diffusion coefficient, from those in the ideally dilute solutions.

This chapter is about semidilute solutions, $c > c^*$. We learn both thermodynamics and dynamics. The properties of semidilute solutions are drastically different from those of dilute solutions. With a mere tenfold increase in the concentration, the osmotic pressure can easily increase by a factor of several hundred. In the ideal solution, in contrast, the osmotic pressure is proportional to $c$. Furthermore, the overall chain motion is slow in semidilute solutions because the chains are entangled: semidilute solutions of a high-molecular-weight polymer can barely flow. The solutions are highly viscous and may even behave like elastic rubber.

The osmotic pressure and the time scale of motion depend heavily on concentration and molecular weight. The dependence is universal for a certain class of solutions; each class, however, exhibits a characteristic dependence. For many years, we had not had a good understanding of those characteristics until the blob concept, the scaling theory, and the reptation model were introduced in 1970s.[44,45] With simple ideas and simple mathematics, these concepts elegantly explained the observed complicated dependence.

Semidilute solution, $c > c^*$, is unique to polymer solutions. Because $c^*$ is low, the semidilute regime extends to a low concentration (in terms of g/L). As we have

seen in Section 1.8, polystyrene of $M = 3 \times 10^5$ g/mol has $c^* \cong 13$ g/L. The upper limit of the semidilute range is sometimes denoted by $c^{**}$. Above $c^{**}$, the monomers are congested and the solution is sometimes called concentrated (it is not a well-defined term). In semidilute solutions, monomers are not congested, but polymer chains have many other chains overlapping them. The chains as a whole are congested, and the interactions between the chains are therefore strong. With a further increase in $c$, the overlaps become more serious. In contrast, in solutions of a low-molecular-weight nonionic compound, the low concentration (in g/L) promises weak interactions between the solute molecules.

The semidilute regime is often specified by $c^* \ll c < c^{**}$. With $c^*$ at around 10 g/L for polystyrene of $M_w = 6 \times 10^5$ g/mol, for instance, and $c^{**}$ at around 300 g/L, the double inequality may appear to impose a severe restriction on the accessibility by an ordinary polymer. In practice, however, solutions several times as concentrated as $c^*$ already qualify as semidilute solutions. With ambiguity in the definition of $c^*$ (Eqs. 1.108–1.110), it does not make sense to ask how high the concentration should be for the solution to be semidilute. As we will see in many experimental results, there is an easy way to find whether or not the concentration is sufficiently high.

In Section 4.2, we will learn about the thermodynamics of semidilute solutions. We will consider linear flexible chains only. The mean-field theory explained in Section 2.2 is assumed to be effective in a whole range of concentrations. The theory, however, fails to explain various experimental results. The failure can be ascribed to the stronger interactions between chain molecules consisting of covalently bonded monomers compared with the mean-field interactions that do not distinguish bonded monomers from nonbonded monomers. Fortunately, the blob model and the scaling theory explain the thermodynamics that characterize semidilute solutions.

Section 4.3 focuses on dynamics. We will first examine the overall concentration fluctuations of highly entangled chains. We will then look at the motions of each chain through the maze of other chains.

In this chapter, we attach the subscript "0" to denote the value of the relevant quantity in the dilute solution limit. For instance, $R_{g0}$ is the root-mean-square radius of gyration, $R_g$, in solutions at sufficiently low concentrations. It may appear strange that the chain size changes with concentration, but, as we will learn in Section 4.2.2, the chain size diminishes because the excluded volume that swells the chains at low concentrations becomes negligible at higher concentrations.

## 4.2 THERMODYNAMICS OF SEMIDILUTE POLYMER SOLUTIONS

### 4.2.1 Blob Model

***4.2.1.1 Blobs in Semidilute Solutions*** In the semidilute solutions, the chains are congested and highly overlapping with other chains, as shown in Figure 4.1a.

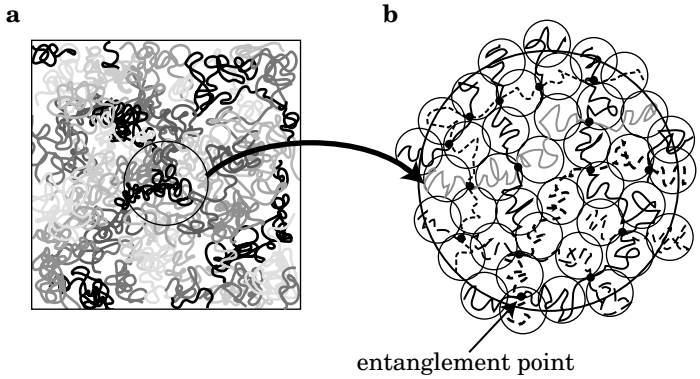


**Figure 4.1.** a: Highly entangled polymer chains in a semidilute polymer solution. b: When zoomed in, the entangled chains can be regarded as consisting of blobs.

Different gray levels are used to distinguish the chains. When zoomed in, the solution would look like Figure 4.1b. The intersections between different chains, indicated by small filled circles, are called **entanglement points**. Between two neighboring entanglement points on the same chain, the chain claims its own territory; there is only a small chance for monomers of other chains to sneak in. We can superimpose a sphere called a **blob** onto this sovereign. The same monopolized territory applies to the other parts of the chain and to other chains as well. In this way, we can fill up the entire solution with blobs.

The blob concept, which was introduced in the 1970s, solved then mysterious problems elegantly.[44] The **blob model** is extremely useful and robust in predicting various static and dynamic properties of the semidilute solutions of polymers. Although limited to power relationships, the blob model allows us to find how these properties depend on the concentration and the molecular weight. In this section, we will first find the blob size in the semidilute solution of polymer chains of a given length at a given concentration. We will then use the blob model to obtain various thermodynamic quantities of the semidilute solution.

***4.2.1.2 Size of the Blob*** Let us first estimate the size of the blob $\xi$ (Fig. 4.2). Each polymer chain consists of $N$ monomers of size $b$. The polymer is monodisperse. For convenience, we use the monomer density $\rho$ defined in Section 2.4.5.2. It is the number of monomers in a unit volume and related to the mass concentration $c$ by

$$\frac{\rho}{N} = \frac{cN_A}{M} \tag{4.1}$$

where $M$ is the molecular weight of the polymer. The two sides express the number of polymer chains in a unit volume.

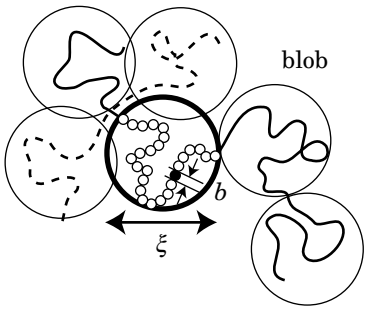


**Figure 4.2.** A blob of size $\xi$ has $g_N$ monomers of size $b$ from the same chain.

At the overlap concentration (defined in Section 1.8), the $N$ monomers in a volume of ${R_{g0}}^3$ give the overall monomer density $\rho^*$:

$$\rho^* = Nc^*N_A/M \cong N{R_{g0}}^{-3} \cong b^{-3}N^{1-3\nu} \quad \text{or} \quad \rho^* \cong b^{-3}N^{-4/5} \tag{4.2}$$

where $R_{g0} \cong bN^{\nu}$ was used. The second equality is for $\nu = 3/5$ in the good solvent. In what follows, we often display the power relationships for a general $\nu$ and $\nu = 3/5$ side by side. If necessary, we can also derive a relevant power relationship for semidilute solutions in the theta condition by setting $\nu = 1/2$ (see Section 4.2.2.6).

The blob size $\xi$ is equal to $R_{g0}$ at $\rho^*$. As the solution becomes more concentrated, the chains become more heavily overlapped with each other. When there are more entanglement points, the blob must decrease its size (Fig. 4.3).

We make two assumptions to estimate the blob size in the semidilute solution at monomer density $\rho$:

(1) Within each blob, the partial chain takes a conformation of the isolated parent chain. Let $g_N$ monomers be in each blob. Then,

$$b{g_N}^{\nu} \cong \xi \qquad \text{or} \qquad b{g_N}^{3/5} \cong \xi \tag{4.3}$$

(2) The blobs occupy the whole volume of the solution without voids. Therefore, the density of monomers in the blob mirrors the density in the whole solution:

$$\rho \cong g_N/\xi^3 \tag{4.4}$$

Combining the two equations, we obtain

$$\xi \cong b^{-1/(3\nu-1)}\rho^{-\nu/(3\nu-1)} \quad \text{or} \quad \xi \cong b^{-5/4}\rho^{-3/4} \tag{4.5}$$

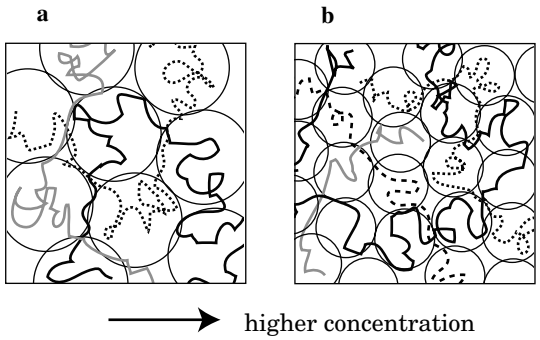


**Figure 4.3.** As the concentration increases, the blob size decreases from the one shown in panel a to the one in panel b.

The negative exponent on $\rho$ tells that the blobs become smaller with an increasing $\rho$. Note also that $\xi$ does not depend on $N$ explicitly. It is determined by the monomer density or the mass concentration only, once the polymer is given.

The blob size relative to $R_{g0}$ is calculated from $\xi^{1-3\nu} \cong b\rho^{\nu} \cong (\rho/\rho^*)^{\nu}\, b(NR_{g0}{}^{-3})^{\nu} \cong (\rho/\rho^*)^{\nu} R_{g0}{}^{1-3\nu}$ as

$$\boxed{\xi \cong R_{g0}(\rho/\rho^*)^{-\nu/(3\nu-1)} \quad \text{or} \quad \xi \cong R_{g0}(\rho/\rho^*)^{-3/4} \quad \text{blob size}} \tag{4.6}$$

Apparently Eq. 4.6 holds only for $\rho > \rho^*$. Below the overlap concentration, the chains are isolated. The blob contains the whole chain and therefore $\xi \cong R_{g0}$. Figure 4.4 illustrates how the blob size decreases with an increasing concentration for three different chain lengths specified by their radii of gyration in the dilute solution limit, $R_{g0}(1)$, $R_{g0}(2)$, and $R_{g0}(3)$. In a solution of polymer chains with $R_{g0}(2)$, $\xi \cong R_{g0}(2)$ at low concentrations. As $\rho$ exceeds its overlap concentration $\rho^*(2)$, $\xi$ approaches a straight line with a slope of $-3/4$. In a solution of the longer chains $[R_{g0}(1)]$, the crossover from a constant at $R_{g0}$ to a slope of $-3/4$ occurs at a lower concentration because its $\rho^*$ is smaller $[\rho^*(1)]$. The straight line they approach at $\rho > \rho^*$ is identical to the straight line that the chains with $R_{g0}(2)$ approach. The curve for the shorter chains $[R_{g0}(3)]$ merges with the same straight line at a higher concentration $\rho^*(3)$. Note that $\xi$ is independent of $N$ in Eq. 4.5.

Once $\xi$ is obtained, $g_N$ is evaluated as follows:

$$g_N \cong \rho\xi^3 \cong (b^3\rho)^{-1/(3\nu-1)} \cong N(\rho/\rho^*)^{-1/(3\nu-1)} \quad \text{or} \quad g_N \cong (b^3\rho)^{-5/4} \cong N(\rho/\rho^*)^{-5/4} \tag{4.7}$$

where Eqs. 4.2, 4.4, and 4.5 were used. At the overlap concentration, $g_N \cong N$ as required. In the blob model, the polymer chain of $N$ monomers is replaced by a chain of $N/g_N \cong (\rho/\rho^*)^{1/(3\nu-1)} \cong (\rho/\rho^*)^{5/4}$ blobs, each consisting of $g_N$ monomers. The number of blobs constituting the polymer chain increases as their size decreases. Note that both $\xi$ and $g_N$ decrease with an increasing $\rho$, but in different exponents.

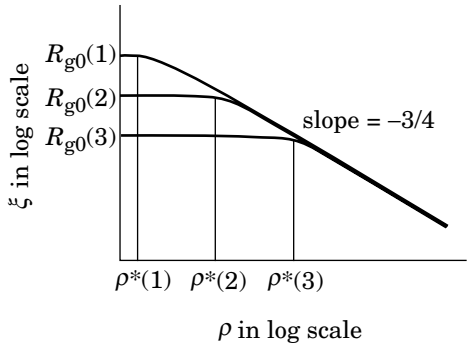


**Figure 4.4.** Blob size $\xi$ plotted as a function of monomer density $\rho$ in a double logarithmic scale for three different chain lengths. Their radii of gyration in the dilute solution limit are $R_{g0}(1)$, $R_{g0}(2)$, and $R_{g0}(3)$. Their overlap concentrations are $\rho^*(1)$, $\rho^*(2)$, and $\rho^*(3)$. In the semidilute solutions, $\xi \sim \rho^{-3/4}$.

The blob is a conceptual object. Unlike $R_{g0}$, we cannot measure the size of the blob. Later, we will derive the identity, *blob size = correlation length*. The latter can be conveniently measured in static and dynamic light scattering.

It is now apparent that there is an upper limit for the concentration range in which the blob model is effective. With an increasing $\rho$, $\xi$ decreases, but it cannot be smaller than $b$, the monomer size. The upper limit of $\rho$, which we denote by $\rho^{**}$, is determined from the condition of $\xi \cong b$. Using Eq. 4.5, $\rho^{**}$ is evaluated as

$$\rho^{**} \cong b^{-3} \tag{4.8}$$

Unlike $\rho^*$, the upper limit is independent of $N$. It is considered that, in real polymer solutions, the volume fraction of the polymer at $\rho^{**}$ is around 0.2–0.3.

With Eq. 4.2, we find

$$\rho^{**}/\rho^* \cong N^{3\nu-1} \quad \text{or} \quad \rho^{**}/\rho^* \cong N^{4/5} \tag{4.9}$$

Thus, the lower limit and the upper limit of the semidilute regime are widely separated, especially when $N \gg 1$. As expected, $g_N \cong 1$ at the upper limit.

***4.2.1.3 Osmotic Pressure*** The osmotic pressure counts the number of independently moving units per volume of the solution. It is one of the colligative properties of the solution. At low concentrations, the whole chain moves as a unit. The center-of-mass displacement is synonymous to a change in the position of the whole chain (in the small wave vector limit). The dilute polymer solution is an ideal solution of $\rho/N = cN_A/M$ solute molecules in a unit volume. The osmotic pressure $\Pi_{ideal}$ of the solution is therefore

$$\Pi_{ideal} = \frac{cN_A}{M} k_B T = \frac{\rho}{N} k_B T \tag{4.10}$$

In the semidilute solution, monomers in a given blob are moving independently of the monomers in the other blobs, at least in a short time scale. Entanglement makes rearrangement of monomers within a blob by far easier and faster compared with the rearrangement of the blobs. The monomers in the blob move more or less together (correlated motion), just as the whole chain moves together at low concentrations. Now in the semidilute solution, the blob is a moving unit. Therefore, the osmotic pressure of the semidilute solution is given as $k_BT \times$ (the number of blobs in a unit volume):

$$\Pi \cong \xi^{-3} k_B T \tag{4.11}$$

With Eq. 4.5, we obtain

$$\boxed{\Pi/k_BT \cong (b\rho^{\nu})^{3/(3\nu-1)} \quad \text{or} \quad \Pi/k_BT \cong b^{15/4}\rho^{9/4} \quad \text{osmotic pressure}} \tag{4.12}$$

In the semidilute solution, $\Pi$ does not depend explicitly on $N$. It is determined by $\rho$ only. Compared at the same mass concentration, solutions of a polymer have the same $\Pi$ regardless of the molecular weight of the polymer. It means that a small volume that contains 1,000 chains of 1,000 monomers is thermodynamically equivalent to the volume that contains 100 chains of 10,000 monomers or 10 chains of 100,000 monomers, as long as the concentration is in the semidilute range. The dependence of $\Pi/(\rho k_BT)$ on $\rho$ is depicted in Figure 4.5 for three different chain lengths. At low concentrations, the solution of the shorter chain claims a higher osmotic pressure because the unit volume of the solution has more moving units. When $\rho \ll \rho^*$, $\Pi/(\rho k_BT)$ is constant at $1/N$. A departure from this ideal-solution behavior occurs at around $\rho^*$. Thus the departure occurs at a lower concentration for the longer chains. In the semidilute solution, the plots of $\Pi/(\rho k_BT)$ for different values of $N$ should overlap with each other and follow a common straight line with

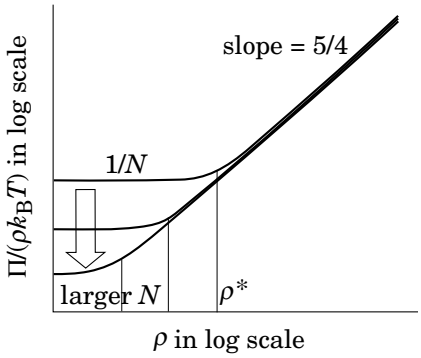


**Figure 4.5.** Osmotic pressure $\Pi$ reduced by $\rho k_BT$ is plotted as a function of monomer density $\rho$ in a double logarithmic scale for three different chain lengths. At low concentrations, $\Pi/(\rho k_BT) = N^{-1}$. In the semidilute solutions, $\Pi/(\rho k_BT) \sim \rho^{5/4}$. The cross over occurs at around $\rho^*$.

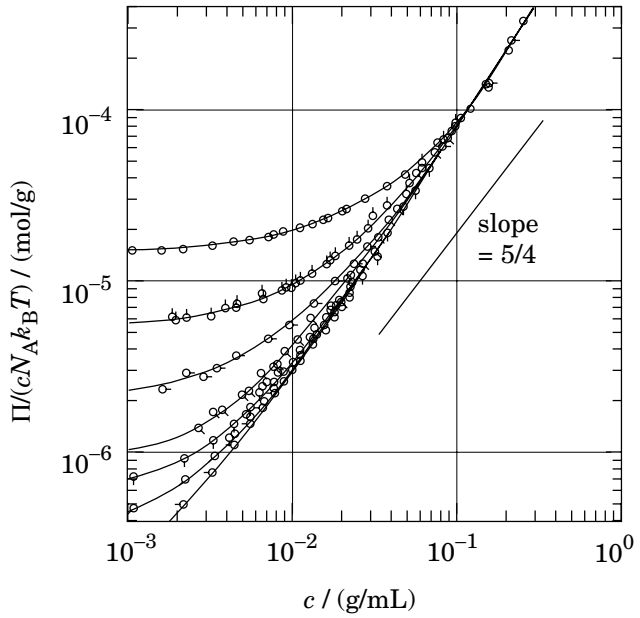


**Figure 4.6.** Osmotic pressure $\Pi$ of poly($\alpha$-methyl styrene) in toluene at 25°C, reduced by $cN_Ak_BT$, plotted as a function of mass concentration $c$ of the polymer. Data were obtained, from top to bottom, for various molecular weights from $7 \times 10^4$ to $7.47 \times 10^6$ g/mol. The solid line has a slope of $5/4$. (From Ref. 46.)

a slope of $5/4$. The shorter chains need a higher concentration for its osmotic pressure to approach the straight line.

Experimental results support the presence of the asymptotic straight line. Figure 4.6 shows the osmotic pressure, reduced by $cN_Ak_BT$, for different molecular weights of poly($\alpha$-methyl styrene) in toluene, measured at 25°C.[46] The vapor pressure osmometry, explained in Appendix 2.A, was used for the measurements. The nearly flat line at low concentrations is seen only for the lowest-molecular-weight fraction. At high concentrations, data obtained for fractions of different molecular weights approach a single straight line with a slope of 1.5, slightly greater than $5/4$, the predicted exponent in the blob model. We will discuss this difference in Section 4.2.2.1.

The ratio of $\Pi$ of the semidilute solution to $\Pi_{\text{ideal}}$ of the ideal solution compared at the same concentration is

$$\boxed{\Pi/\Pi_{\text{ideal}} \cong (\rho/\rho^*)^{1/(3\nu-1)} \quad \text{or} \quad \Pi/\Pi_{\text{ideal}} \cong (\rho/\rho^*)^{5/4}} \tag{4.13}$$

where Eq. 4.2 was used. In the semidilute solution, $\rho/\rho^*$ can be large. Then the osmotic pressure is much greater than the one we would expect for the ideal solution of the same concentration. When equilibrated with a pure solvent through a semipermeable membrane that passes solvent molecules only, the semidilute solution will suck in a large amount of solvent.

***4.2.1.4 Chemical Potential*** We find here how the excess chemical potential $\delta\mu$ depends on $\rho$, where $\delta\mu$ is the difference of the chemical potential $\mu$ from the chemical potential in the ideal solution of the same concentration. We note that $\delta\mu$ is calculated from the nonideal part of the free energy. In the semidilute solution, it is approximately given by $\Pi V$, where $\Pi$ is given by Eq. 4.12. Because $\rho V/N$ is the number of polymer chains in volume $V$, $\delta\mu$ is obtained as

$$\delta\mu \cong \left(\frac{\partial(\Pi V)}{\partial(\rho V/N)}\right)_V = N\left(\frac{\partial\Pi}{\partial\rho}\right)_V \cong Nk_BTb^{3/(3\nu-1)}\rho^{1/(3\nu-1)} \tag{4.14}$$

We can rewrite $\delta\mu$ into a dimensionless quantity:

$$\boxed{\delta\mu/k_BT \cong (\rho/\rho^*)^{1/(3\nu-1)} \quad \text{or} \quad \delta\mu/k_BT \cong (\rho/\rho^*)^{5/4} \qquad \begin{matrix}\text{excess chemical}\\ \text{potential}\end{matrix}} \tag{4.15}$$

The right-hand side is identical to that of Eq. 4.13, as expected.

The following equation can be used for the overall chemical potential $\mu$. It is an approximate formula valid from dilute to semidilute solutions:

$$(\mu - \mu^\circ)/k_BT \cong \ln\phi + a_\mu(\phi/\phi^*)^{1/(3\nu-1)} \quad \text{or} \quad \ln\phi + a_\mu(\phi/\phi^*)^{5/4} \tag{4.16}$$

with $\mu^\circ$ is the chemical potential at an appropriate reference state, and $a_\mu$ is a constant independent of $N$. Equation 4.16 uses the volume fraction $\phi$ and the overlap volume fraction $\phi^*$, but we can use $\rho$ and $\rho^*$ or $c$ and $c^*$ as well.

Figure 4.7 depicts $\mu/k_BT$ for three different chain lengths. At low concentrations, the solution is ideal. As $\rho$ exceeds $\rho^*$, $\mu$ deviates upward. The deviation occurs at a lower concentration for the longer chain, and the deviation is more serious, compared with the shorter chain at the same $\rho$.

As we have seen in this subsection, the blob model does not give an estimate of the missing numerical coefficient. Often, our interest is to find the power relationship only, however. Then, the blob model is a powerful tool.

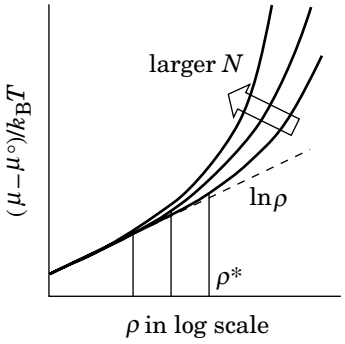


**Figure 4.7.** Chemical potential $\mu$, plotted as a function of monomer density $\rho$ for three different chain lengths.

### 4.2.2 Scaling Theory and Semidilute Solutions

***4.2.2.1 Scaling Theory*** In the preceding subsection, we employed a blob model to derive power relationships for various thermodynamic quantities that characterize the semidilute solutions. The simple assumption produced useful results that agree with those obtained in experiments. We can derive the same results without assuming a blob. We will use the **scaling theory** here for that purpose.

The scaling theory has been successfully used to explain critical phenomena. The latter are about an often drastic change in physical quantities as the system approaches the order-disorder transition point. Well-known examples include ferromagnet–paramagnet phase transition in magnets and nematic–isotropic phase transition in liquid crystals. The demixing transition near the UCST and LCST in a blend of two liquids also belongs to the order-disorder transition. The system changes from the disordered phase to the ordered phase as the temperature $T$ approaches the critical temperature $T_c$. Deep in the disordered phase, the system is uniform and structureless. As $T$ approaches $T_c$, fluctuations grow in the local magnetization, the local alignment of the liquid crystalline molecules, or the local composition of the two-component liquid. Increasingly larger domains develop with a partially ordered structure. At $T = T_c$, the domain size becomes infinite, and the whole system separates into macroscopically ordered phase. In the demixing of two liquids, the system separates into two macroscopic domains. It is known that at near $T_c$ the domain size grows in a power of the temperature difference $|T - T_c|$.

The scaling theory has been successfully applied to polymer systems by drawing analogy between $T - T_c \to 0$ and $N^{-1} \to 0$. Increasing the chain length is equivalent to approaching $T_c$. Together with the blob model, the theory has been particularly instrumental in elucidating the thermodynamics and dynamics of the semidilute polymer solutions. Since its initiation by de Gennes in the 1970s, applications of this theory have proliferated.[44] The scaling theory has become a common language in polymer science. To apply the scaling theory to our own polymer systems, we do not need to know the details of the mathematics behind the theory; however, we can still obtain illuminating results from the application, as we will see below.

Let us first consider the osmotic pressure $\Pi$. The virial expansion of $\Pi$ reduced by $\Pi_{ideal}$ needs to be a power series of the dimensionless concentration of the polymer chains, $\rho R_{g0}^3/N$:

$$\frac{\Pi}{k_B T} = \frac{\rho}{N}[1 + \text{const.} \times (\rho R_{g0}^3/N) + \text{const.} \times (\rho R_{g0}^3/N)^2 + \cdots] \qquad (4.17)$$

Note that $\rho R_{g0}^3/N$ is equal to the reduced concentration $\rho/\rho^* = \phi/\phi^* = c/c^*$. In general, the factor in the square bracket of Eq. 4.17 is a universal function of $\rho R_{g0}^3/N$ defined for $\rho R_{g0}^3/N \geq 0$. By "universal," we mean that the functional form is independent of $N$ or $b$ except through $\rho R_{g0}^3/N$. Therefore, different polymer–solvent combinations share a common function, as along as the solvent is good to the polymer or the polymer chain follows the same statistics. The universal

function is called a **scaling function**. We express it by $f_\Pi$:

$$\frac{\Pi}{k_B T} = \frac{\rho}{N} f_\Pi(\rho {R_{g0}}^3/N) \tag{4.18}$$

Note that a dimensionless quantity $N\Pi/(\rho k_B T)$ is equated to another dimensionless quantity $f_\Pi(x)$ with $x = \rho {R_{g0}}^3/N$.

As $x \to 0$, $f_\Pi(x)$ approaches unity, that is, the solution is ideal in the dilute-solution limit. The scaling theory assumes that $f_\Pi(x)$ for large $x$ asymptotically approaches a power of $x$ with a **scaling exponent** $m$ yet to be determined. Thus,

$$f_\Pi(x) \begin{cases} = 1 & (x \to 0) \\ \cong x^m & (x \gg 1) \end{cases} \tag{4.19}$$

In the semidilute solution ($x \gg 1$),

$$\frac{\Pi}{k_B T} \cong \frac{\rho}{N} (\rho {R_{g0}}^3/N)^m \cong b^{3m} \rho^{1+m} N^{m(3\nu-1)-1} \tag{4.20}$$

In a solution of highly overlapped chains, the thermodynamic properties do not explicitly depend on $N$ but on $\rho$ only, as the result of the blob model indicates. From the condition that $\Pi/k_B T$ be independent of $N$, we determine $m$ as $m = 1/(3\nu - 1)$ or $m = 5/4$, and Eq. 4.20 becomes identical to Eq. 4.12. Without assuming the blobs, we derived an expression for $\Pi$ that is identical to the one we obtained earlier in the blob model. This identity is already a proof for the blob model.

It is apparent in Eq. 4.20 that only a power of $x$ for $f_\Pi(x)$ can make $\Pi$ independent of $N$. Although we assumed the power dependence, it is rather a prerequisite for the independence of $N$.

As in the blob model, the scaling theory does not provide an estimate of the numerical coefficient missing in Eq. 4.19. The theory tells only that $f_\Pi(x) \sim x^{5/4}$ when $x \gg 1$. If needed, we can find the exact relationship in experiments or computer simulations with the help of the scaling prediction. Often, the renormalization group theory can provide the missing coefficient.

It is natural to expect that $f_\Pi(x)$ shows a smooth crossover from 1 at $x \ll 1$ to $x^{5/4}$ at $x \gg 1$. The scaling function can be displayed by plotting $\Pi/\Pi_{ideal} = \Pi M/(cRT)$ as a function of $\rho/\rho^* = c/c^*$. This type of plot is called a **scaling plot**. The three curves in Figure 4.5 can be superimposed on top of the other by rescaling the abscissa and the ordinate and therefore by translating the three curves vertically and horizontally, as shown in Figure 4.8. The overlapped curve is called a **master curve**.

The scaling function obtained in the renormalization group theory by Ohta and Oono[47] has the same power relationship at $\rho \gg \rho^*$ as that of Eq. 4.19. They proposed an interpolation formula:

$$\Pi/\Pi_{ideal} = 1 + \tfrac{1}{2} X \exp\left\{\tfrac{1}{4}[X^{-1} + (1 - X^{-2}) \ln(1 + X)]\right\} \tag{4.21}$$

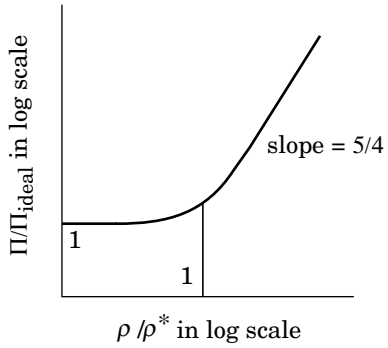


**Figure 4.8.** Scaling plot for the osmotic pressure. The reduced osmotic pressure $\Pi/\Pi_{ideal}$ is plotted as a function of the reduced concentration $\rho/\rho^*$ in a double logarithmic scale. The scaling function changes smoothly from unity at $\rho/\rho^* \ll 1$ to a slope of $5/4$ at $\rho/\rho^* \gg 1$.

where $X = (16/9)A_2Mc$. The latter is another way to scale the concentration into a reduced quantity. We can use $X = 3.49 \times c/c^*$ as well.

A master curve was obtained for the data shown in Figure 4.6 by rescaling both the abscissa and the ordinate for each set of the data. The definition of $c^*$ by Eq. 1.108 was employed. In Figure 4.9, data obtained for different molecular weights of the polymer lie on a master curve.[46] At sufficiently high concentrations,

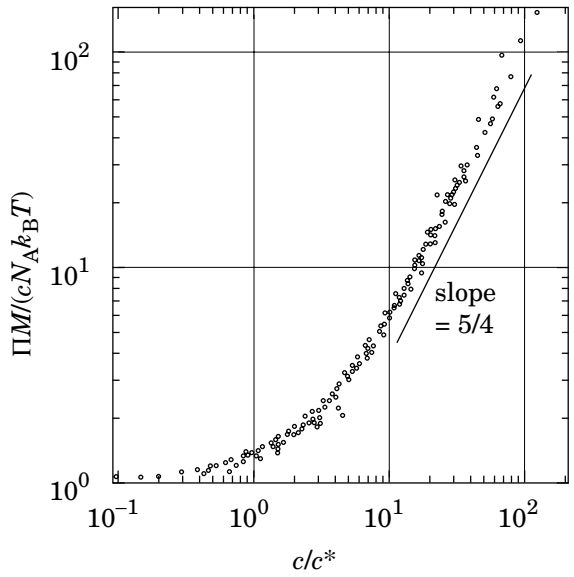


**Figure 4.9.** Scaling plot for the osmotic pressure for the data shown in Figure 4.6. The reduced osmotic pressure $\Pi M/(cN_Ak_BT)$ is plotted as a function of the reduced concentration $c/c^*$. The solid line has a slope of $5/4$. (From Ref. 46.)

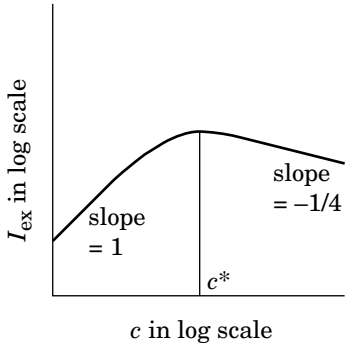


**Figure 4.10.** Excess scattering intensity $I_{ex}$ of a polymer solution peaks at around $c^*$. In the dilute solution, $I_{ex} \sim c$. In the semidilute solution, $I_{ex} \sim c^{-1/4}$.

the curve runs along a straight line with a slope of $5/4$. Compared with Figure 4.6, the agreement with the scaling prediction is better because in the scaling plot the data obtained for the higher-molecular-weight fractions dominate the range of $c/c^* \gg 1$. In Figure 4.6, in contrast, the asymptotic curve is drawn for the data at large values of $c$ obtained for low-molecular-weight fractions. Whether the master curve is obtained from the experimental results and whether the same exponent as the theoretical prediction is obtained gives a final word to the soundness of the blob model and the assumption that $\Pi$ is independent of $N$ in the semidilute solution.

***4.2.2.2 Osmotic Compressibility*** In Section 2.4, we learned that the molecular weight and concentration-dependent factor in the excess scattering intensity $I_{ex}$ of the polymer solution is $c/(\partial\Pi/\partial c)$. The denominator is the osmotic compressibility. See Eqs. 2.104–2.107. At low concentrations, $\partial\Pi/\partial c = N_A k_B T/M$, and therefore $I_{ex} \sim c$. In the semidilute solution, $\partial\Pi/\partial c \sim c^{5/4}$, and therefore $I_{ex} \sim c^{-1/4}$. Figure 4.10 shows a sketch for $I_{ex}$. The intensity peaks at around $c^*$. There is a crossover from $c$ to $c^{-1/4}$ as $c$ exceeds $c^*$.

Conversely, $I_{ex}$ should provide an estimate of $\partial\Pi/\partial c$. Another master curve should be obtained when $(M/N_A k_B T)(\partial\Pi/\partial c)$, estimated in light-scattering experiments, is plotted as a function of $c/c^*$ (Problem 4.2). Furthermore, the master curve in the double logarithmic plot should asymptotically run along a straight line with a slope of $5/4$ at $c/c^* \gg 1$. These properties were verified in experiments. Figure 4.11 compiles data obtained for different molecular weights of polystyrene in toluene and methyl ethyl ketone.[48] The reduced osmotic compressibility $(M/N_A k_B T)(\partial\Pi/\partial c)$ is plotted as a function of $(16/9)A_2 Mc$. It is easy to draw a master curve that runs in the middle of the scattered experimental data. The master curve approaches unity in the low concentration limit and adopts a slope of $5/4$ in the semidilute regime, in agreement with the scaling prediction.

***4.2.2.3 Correlation Length and Monomer Density Correlation Function*** We now apply the scaling theory to the correlation length $\xi$ of local monomer density

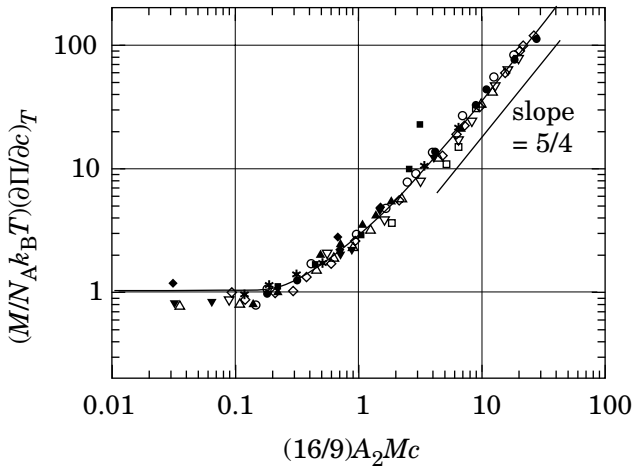


**Figure 4.11.** Reduced osmotic compressibility, $(M/N_A k_B T)(\partial\Pi/\partial c)_T$, plotted as a function of $(16/9)A_2Mc$ in a double logarithmic scale, obtained in the static light-scattering experiments for solutions of polystyrene of various molecular weights in toluene and methyl ethyl ketone. (From Ref. 48.)

fluctuations in solution. The symbol is the same as the one we used for the blob size. In fact, we will find here that *correlation length* ≅ *blob size.*

A homogeneous solution of polymer is not exactly uniform to the length scale of the monomer size. Connectivity of monomers gives rise to a nonuniform distribution of monomer density in the neighborhood of a given monomer. At low concentrations, the chains are well separated. The local density is higher in the neighborhood of a given monomer than it is away from the polymer chain, as we learned in Section 2.4.6. The nonuniform local density distribution persists in the semidilute solution as well. Figure 4.12a depicts polymer chains in the semidilute polymer solution. Figure 4.12b shows the monomer density profile along the solid line in panel a. The density fluctuates but not completely randomly. When $\rho$ is above the average at one spot, the tendency persists for some distance $\xi$. This distance is called a correlation length.

We learned in Section 2.4.6 that $\xi \cong R_{g0}$ at low concentrations. As the chains overlap in the semidilute solution, the correlation in the density fluctuations over the distance of $R_{g0}$ is quickly lost, and the correlation length becomes shorter. We introduce another scaling function $f_\xi(x)$ and write

$$\xi = R_{g0} f_\xi(x) \quad \text{with} \quad f_\xi(x) \begin{cases} = 1 & (x \to 0) \\ \cong x^u & (x \gg 1) \end{cases} \tag{4.22}$$

where $x = \rho/\rho^*$. We expect the scaling exponent $u$ to be negative. In terms of $b$, $N$, and $\rho$, $\xi$ is expressed as

$$\xi \cong b^{1+3u} N^{\nu+u(3\nu-1)} \rho^u \tag{4.23}$$

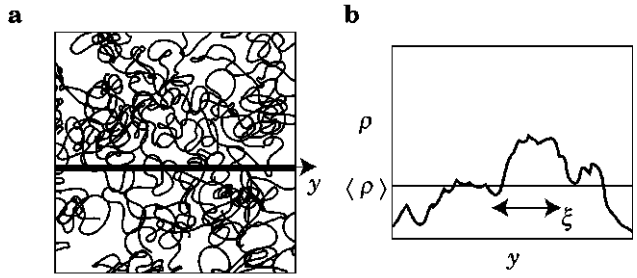


**Figure 4.12.** a: Polymer chains in semidilute solution. b: The density profile along the straight line in panel a.

Again, we impose that $\xi$ be independent of $N$ when $\rho/\rho^* \gg 1$. The condition is given as $\nu + u(3\nu - 1) = 0$, i.e., $u = -\nu/(3\nu - 1)$ or $u = -3/4$. Thus, we find the correlation length decreases with an increasing concentration in a power law with an exponent of $-3/4$. The dependence is exactly the same as the one given by Eq. 4.6 for the blob size. Thus, the blob is essentially a sphere with a diameter equal to the correlation length. It indicates that the monomers within a blob move cooperatively and motions of monomers in different blobs are not correlated with each other.

The scaling plot for $\xi/R_{g0}$ is shown schematically in Figure 4.13. It was prepared by translating the three curves in Figure 4.4 vertically and horizontally.

The correlation length of the polymer solution can be estimated in the static light scattering. Here, we use the **Ornstein-Zernike correlation function** $g_{OZ}(\mathbf{r})$ to find $\xi$ experimentally. This correlation function is often used for the correlation $\langle \Delta\rho(\mathbf{r})\Delta\rho(0)\rangle/\rho$ of the density fluctuation $\Delta\rho(\mathbf{r}) = \rho(\mathbf{r}) - \langle\rho\rangle$ in the semidilute polymer solution. The function is expressed as

$$g_{OZ}(r) = \frac{A}{4\pi\xi^2 r}\exp(-r/\xi) \qquad \text{Ornstein-Zernike correlation function} \tag{4.24}$$

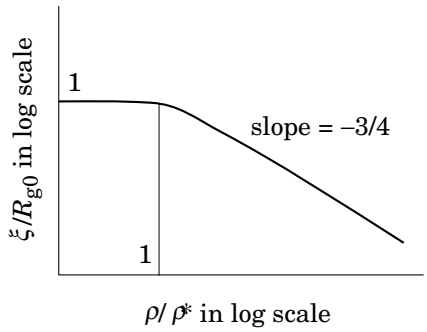


**Figure 4.13.** Scaling plot for the correlation length $\xi$. The reduced correlation length $\xi/R_{g0}$ is plotted as a function of the reduced concentration $\rho/\rho^*$ in a double logarithmic scale.

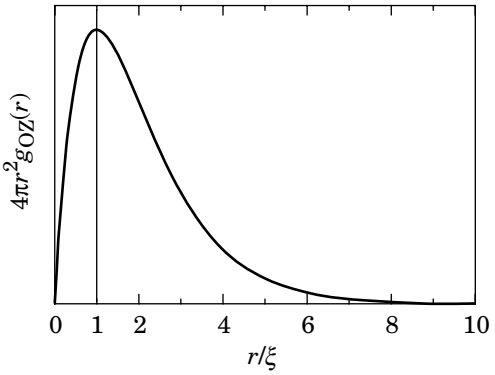


**Figure 4.14.** Ornstein-Zernike monomer density autocorrelation function $g_{OZ}(r)$. The other monomers are most likely found at $r = \xi$.

where $r = |\mathbf{r}|$, and $A$ is a constant to be determined later. It has a singularity at $r = 0$, but it disappears on integration. Figure 4.14 shows a plot of $4\pi r^2 g_{OZ}(r)$. The excess probability of finding other monomers at the distance between $r$ and $r + dr$ from a given monomer is given by $4\pi r^2 g_{OZ}(r)\, dr$. The plot peaks at $r = \xi$. The other monomers are most likely found at $r = \xi$.

The static structure factor $S(\mathbf{k})$ for this correlation function is simple:

$$S(\mathbf{k}) = \int \exp(i\mathbf{k}\cdot\mathbf{r}) g_{OZ}(\mathbf{r})\, d\mathbf{r} = \frac{A}{1 + \xi^2\mathbf{k}^2} \tag{4.25}$$

The reciprocal of $S(\mathbf{k})$ is plotted as a function of $\mathbf{k}^2$ in Figure 4.15. The plot is a straight line with a slope of $\xi^2$. Because $S(\mathbf{k})$ is proportional to the excess scattering intensity at $\mathbf{k}$, we can use this plot to find $\xi$ in the scattering experiments.

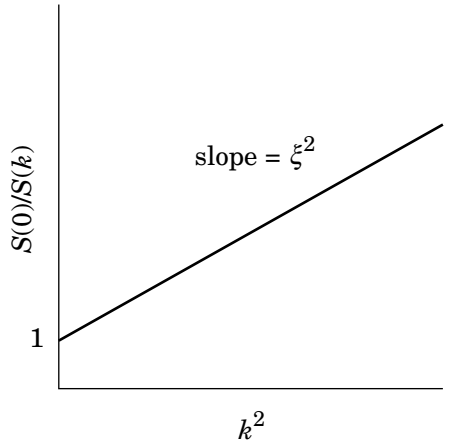


**Figure 4.15.** The reciprocal of the static structure factor $S(k)$ plotted as a function of $k^2$. The slope of the plot is equal to the square of the correlation length $\xi$.

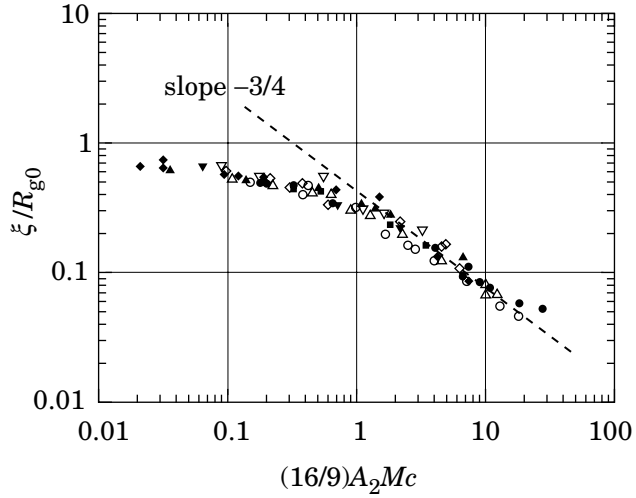


**Figure 4.16.** Scaling plot for the correlation length $\xi$ evaluated in static light-scattering measurements for solutions of polystyrene in toluene and methyl ethyl ketone. The reduced correlation length $\xi/R_{g0}$ is plotted as a function of $(16/9)A_2Mc$ in a double logarithmic scale. The dashed line has a slope of $-3/4$. (From Ref. 48.)

The constant $A$ in $g_{OZ}(\mathbf{r})$ is determined as follows. $V^{-1}\psi_{cc}(\mathbf{k})$ is the Fourier transform of $\langle \Delta c(\mathbf{r})\Delta c(0)\rangle$ (see Eq. 2.105), as $\rho S(\mathbf{k})$ is the Fourier transform of $\langle \Delta\rho(\mathbf{r})\Delta\rho(0)\rangle$ (see Eq. 2.64; a constant term that results in the forward scattering is eliminated here). Together with $c(\mathbf{r}) \propto \rho(\mathbf{r})$, we find

$$\frac{S(0)}{\psi_{cc}(0)} = \frac{\rho}{c^2 V} \tag{4.26}$$

Then,

$$A = S(0) = \frac{\rho k_B T}{c}\frac{\partial c}{\partial \Pi} = N\frac{N_A k_B T}{M}\frac{\partial c}{\partial \Pi} \tag{4.27}$$

where Eqs. 2.106 and 2.107 were used.

The correlation length $\xi$ estimated in static light-scattering experiments is plotted in Figure 4.16 in the scaling plot.[48] The reduced concentration is $(16/9)A_2Mc$. Data obtained for polystyrene fractions of different molecular weights in toluene and methyl ethyl ketone fall on a single master curve. At $(16/9)A_2Mc \gg 1$, the data lie along a straight line with a slope of $-3/4$, in agreement with the scaling prediction. Note that the low concentration limit of $\xi/R_{g0}$ is not unity but $3^{-1/2}$ because the single-chain structure factor is $S_1(\mathbf{k}) = N/(1 + \mathbf{k}^2 R_{g0}{}^2/3)$, that is, $\xi = R_{g0}/3^{1/2}$ at low concentrations (Eq. 2.75).

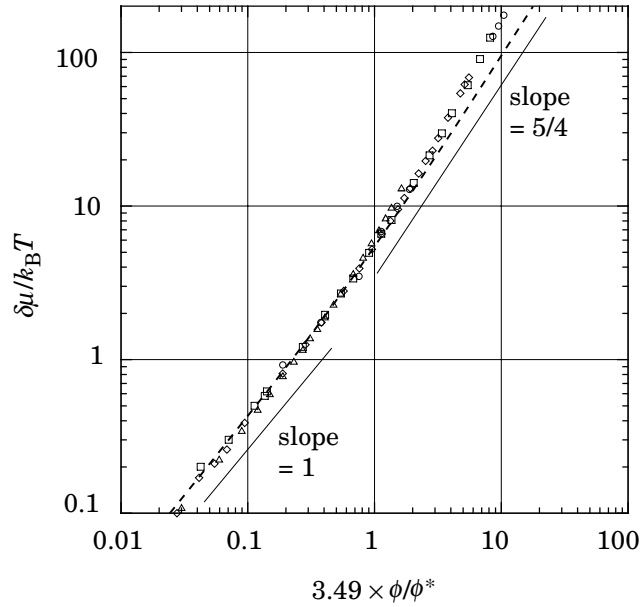


**Figure 4.17.** Scaling plot for the excess chemical potential $\delta\mu$ plotted as function of the reduced concentration, $3.49 \times \phi/\phi^*$. Data were obtained in lattice Monte Carlo simulation for self-avoiding walks of $N = 25$, 100, 200, and 300 on a cubic lattice. The dashed line is by the Ohta-Oono formula. (From Ref. 5.)

***4.2.2.4 Chemical Potential*** The excess chemical potential $\delta\mu(c)$ at concentration $c$ can be obtained from the reduced osmotic pressure $\Pi(c)/\Pi_{\text{ideal}}(c)$ as (Problem 4.4)

$$\frac{\delta\mu(c)}{k_BT} = \frac{\Pi(c)}{\Pi_{\text{ideal}}(c)} - 1 + \int_0^c x^{-1}[\Pi(x)/\Pi_{\text{ideal}}(x) - 1]\,dx \tag{4.28}$$

Another expression of the concentration such as $\rho$ or $\phi$ can be used in place of $c$.

It can be shown that $\delta\mu$ is a function of $c/c^*$ (Problem 4.5). At $c \ll c^*$, the virial expansion of $\Pi(c)$, $\Pi(c)/\Pi_{\text{ideal}}(c) = 1 + A_2Mc + \cdots$, gives $\delta\mu \sim c$. At $c \gg c^*$, $\Pi(c)/\Pi_{\text{ideal}}(c) \sim c^{5/4}$; therefore, $\delta\mu \sim c^{5/4}$ as well. Data for $\delta\mu/k_BT$ obtained for different chain lengths should be on a master curve when plotted as a function of $c/c^*$. Figure 4.17 shows $\delta\mu/k_BT$ evaluated in the Monte Carlo simulation on a cubic lattice for self-avoiding walks of $N = 25$, 100, 200, and 300.[5] As we see, the data are on a master curve. At $\phi \ll \phi^*$, the master curve runs along a straight line with a slope of 1. At $\phi \gg \phi^*$, the master curve runs along a straight line, but the slope is slightly greater than 5/4, the value predicted in the scaling theory. The dashed line was calculated by using Eq. 4.21 with a slight modification[50] (0.3089 in place of 1/4) and Eq. 4.28.

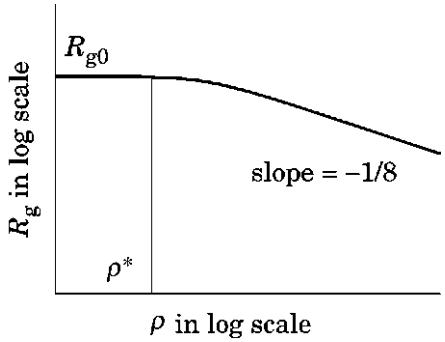


**Figure 4.18.** The polymer chain contracts with an increasing concentration because of shielding of excluded volume. The radius of gyration $R_g$ decreases in a power of monomer density $\rho$ with an exponent of $-1/8$.

***4.2.2.5 Chain Contraction*** Over a length greater than $\xi$, monomer concentration is nearly uncorrelated. A monomer on a given polymer chain will not interact with other monomers on the same chain but in different blobs. In other words, a blob will not feel the presence of other blobs that belong to the same chain. The excluded volume is predominantly between blobs belonging to different chains. Thus, the excluded volume effect that swells the polymer chain at low concentrations is absent over the length beyond $\xi$. This **shielding of the excluded volume** changes the chain statistics drastically.

In the semidilute solution, blobs do not feel the excluded volume by the other blobs. Therefore, a chain of blobs takes a conformation of an ideal chain consisting of $N/g_N$ blobs of size $\xi$. Its radius of gyration $R_g$ in the semidilute solution at monomer density $\rho$ is estimated as

$$R_g^2 \cong (N/g_N)\xi^2 \cong R_{g0}^2(\rho/\rho^*)^{-(2\nu-1)/(3\nu-1)} \quad \text{or} \quad (\rho/\rho^*)^{-1/4} \tag{4.29}$$

where Eqs. 4.6 and 4.7 were used. The polymer chain is swollen in the dilute solution because of the excluded volume, but shrinks in the semidilute solution. The contraction factor for $R_g$ is

$$R_g/R_{g0} \cong (\rho/\rho^*)^{-(\nu-1/2)/(3\nu-1)} \quad \text{or} \quad (\rho/\rho^*)^{-1/8} \tag{4.30}$$

The same contraction factor applies to $R_F$. Figure 4.18 illustrates the contraction in the scaling plot.

In terms of $b$, $N$, and $\rho$, $R_g^2$ is expressed as

$$R_g^2 \cong (b\rho^{1-2\nu})^{1/(3\nu-1)}N \quad \text{or} \quad (b\rho^{-1/5})^{5/4}N \tag{4.31}$$

In the semidilute solution, $R_g \sim N^{1/2}$, the same as the ideal chain. The chain keeps contracting with an increasing $\rho$ by effectively decreasing the monomer size of the

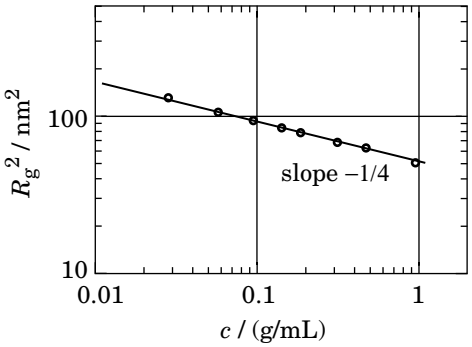


**Figure 4.19.** Reduced mean square radius of gyration, $R_g^2$, of polystyrene in carbon disulfide, plotted as a function of the polymer concentration $c$. Data were obtained in small-angle neutron scattering. The straight line has a slope of $-1/4$. (From Ref. 49.)

ideal chain while holding the relationship of $R_g \sim N^{1/2}$. At $\rho = \rho^{**}$, $\rho \cong b^{-3}$, and $R_g \cong bN^{1/2}$, the same as $R_g$ of the ideal chain of monomer size $b$.

The chain contraction was verified in small-angle neutron-scattering experiments.[49] A mixture of hydrogenated polystyrene (h-PS) and deuterated polystyrene (d-PS) with an equal degree of polymerization (at around 1,100) was dissolved in carbon disulfide. The concentration of d-PS was changed in a wide range, whereas the concentration of h-PS was held low. Thus, the radius of gyration of each h-PS in a matrix of d-PS in the semidilute solution could be measured. Figure 4.19 shows $R_g^2$ as a function of polymer concentration $c$. The data are on a straight line with a slope of $-1/4$, in agreement with the scaling theory. The same power dependence is observed in the range of concentrations that exceeds $c^{**}$.

Lattice computer simulation also verified the scaling relationship.[5] Figure 4.20 shows the scaling plot for four different chain lengths of self-avoiding walks on the cubic lattice. The data plotted as a function of reduced concentration $\phi/\phi^*$ are on a single master plot given by

$$R_g/R_{g0} = [1 + 0.96403(\phi/\phi^*) + 0.34890(\phi/\phi^*)^2]^{-1/16} \tag{4.32}$$

This equation has an asymptote identical to Eq. 4.30, but the scaling exponent of $-1/8$ is not reached in the range shown. Apparently, longer chains are needed to observe the exponent.

***4.2.2.6 Theta Condition*** We can apply all of the relationships that we obtained in the preceding section and the present section to semidilute solutions of a polymer in the theta condition by setting $\nu = 1/2$. We list the relationships in Table 4.1 together with the results for the good solvent.

At the upper limit of the semidilute regime, there will be little distinction between the good solvent and the theta solvent, as the excluded volume is shielded

**TABLE 4.1 Properties of Semidilute Solutions†**

| | General | With $\nu = 3/5$ | With $\nu = 1/2$ |
|---|---|---|---|
| $\Pi/k_BT$ | $(b\rho^{\nu})^{3/(3\nu-1)}$ | $b^{15/4}\rho^{9/4}$ | $b^6\rho^3$ |
| $\Pi/\Pi_{ideal}$ | $(\rho/\rho^*)^{1/(3\nu-1)}$ | $(\rho/\rho^*)^{5/4}$ | $(\rho/\rho^*)^2$ |
| $\delta\mu/k_BT$ | $(\rho/\rho^*)^{1/(3\nu-1)}$ | $(\rho/\rho^*)^{5/4}$ | $(\rho/\rho^*)^2$ |
| $\xi/R_{g0}$ | $(\rho/\rho^*)^{-\nu/(3\nu-1)}$ | $(\rho/\rho^*)^{-3/4}$ | $(\rho/\rho^*)^{-1}$ |
| $R_g/R_{g0}$ | $(\rho/\rho^*)^{-(\nu-1/2)/(3\nu-1)}$ | $(\rho/\rho^*)^{-1/8}$ | $(\rho/\rho^*)^0$ |
| $D_{coop}/D_0$ | $(\rho/\rho^*)^{\nu/(3\nu-1)}$ | $(\rho/\rho^*)^{3/4}$ | $(\rho/\rho^*)^1$ |

†$\rho/\rho^*$ can be replaced with $c/c^*$ or $\phi/\phi^*$.

to the length of the monomer size. All thermodynamic quantities will be the same between the two solvent conditions. Note that the semidilute range is narrower in the theta solvent compared with the good solvent. The solution in the theta solvent becomes nearly identical to the solution in the good solvent by changing its thermodynamics more quickly with an increasing concentration. For instance, the dependence of $\xi$ on the concentration is steeper compared with the good solvent condition. Figure 4.21 compares $\xi/b$ in the good solvent and in the theta solvent. We can draw a similar sketch for other thermodynamic quantities. In the theta solvent, the chain dimension is unchanged from that in the dilute solution limit, as required.

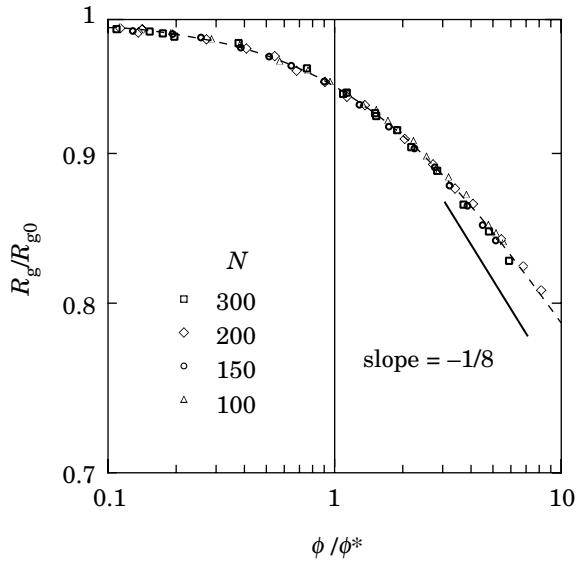


**Figure 4.20.** Scaling plot for $R_g/R_{g0}$ plotted as a function of the reduced concentration $\phi/\phi^*$. The data were obtained in the lattice Monte Carlo simulation for self-avoiding walks. The dashed line represents the best fit by a curve that is identical to the scaling prediction at $\phi/\phi^* \gg 1$. (From Ref. 5.)

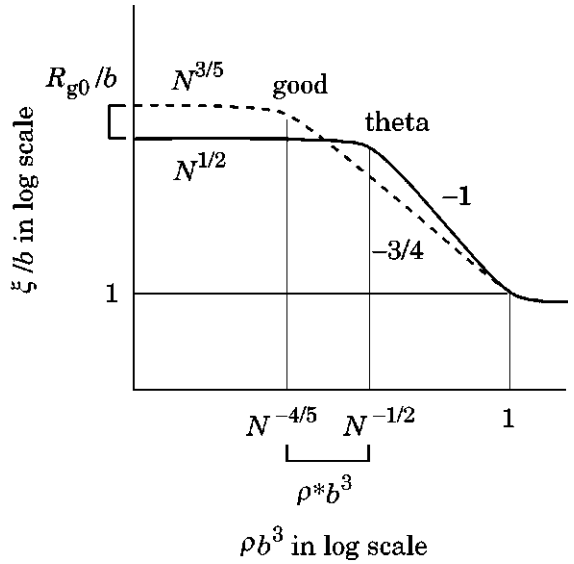


**Figure 4.21.** Comparison of the correlation length $\xi$ in the good solvent (dashed line) and in the theta solvent (solid line). As the monomer density reaches $\rho^{**}$ ($b^3\rho^{**} \cong 1$), the distinction between the two solvent conditions nearly disappears.

### 4.2.3 Partitioning with a Pore

***4.2.3.1 General Formula*** Another phenomenon that exhibits a marked departure from the dilute solution is partitioning of polymer solutions with a small pore. The partitioning rule (size-exclusion principle), which was discussed in Section 2.5, applies to dilute solutions only, in which each polymer chain interacts with the pore independently of other chains. As soon as the chain feels the presence of nearby chains, the rule changes. Here, we apply the results of the scaling theory to consider the change. For simplicity, we adopt $\nu = 3/5$ here.

A solution that contains a polymer at a volume fraction $\phi_E$ is in contact with a pore of diameter $d$. The pore walls are neutral to the polymer, that is, the pore does not have an attractive or repulsive interaction other than the excluded volume (polymers cannot intersect the pore wall). At equilibrium, the polymer volume fraction is $\phi_I$ in the pore. We allow $\phi_I$ and $\phi_E$ to be anywhere from dilute to semidilute regimes. Except near the pore–exterior boundary, $\phi_I$ is uniform along the pore (Fig. 4.22).

We adopt Eq. 4.16 for the chemical potential $\mu_E$ of the chain exterior to the pore:

$$\mu_E/k_BT = \mu^\circ/k_BT + \ln\phi_E + a_\mu(\phi_E/\phi^*)^{5/4} \tag{4.33}$$

Within the pore, the polymer chain has an extra term due to confinement (see Eq. 2.142):

$$\mu_I/k_BT = \mu^\circ/k_BT + \ln\phi_I + a_\mu(\phi_I/\phi^*)^{5/4} + a_c(R_{g0}/d)^{5/3} \tag{4.34}$$

where $a_c$ is another numerical coefficient.

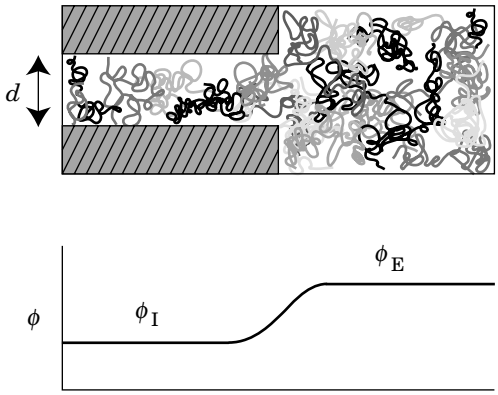


**Figure 4.22**. Partitioning of a semidilute polymer solution with a pore. The concentration profile is shown in the bottom panel.

We neglect the effect of chain contraction at high concentrations. Although the chain contraction decreases the confinement entropy, its effect is usually small (Problem 4.9). Therefore, we also use the confinement entropy of a single chain in the low concentration limit, $k_B a_c (R_{g0}/d)^{5/3}$, for the semidilute solution.

Equating the above two chemical potentials for equilibrium, we obtain

$$\ln \phi_I + a_\mu (\phi_I/\phi^*)^{5/4} + a_c (R_{g0}/d)^{5/3} = \ln \phi_E + a_\mu (\phi_E/\phi^*)^{5/4} \tag{4.35}$$

We evaluate the partition coefficient $K = \phi_I/\phi_E$ in the two concentration regimes.

***4.2.3.2 Partitioning at Low Concentrations*** In the low concentration limit ($\phi_I/\phi^* < \phi_E/\phi^* \ll 1$), the interaction terms can be dropped. We obtain the partition coefficient $K_0$ as $\ln K_0 \cong -(R_{g0}/d)^{5/3}$ (Eq. 2.142).

With an increasing $\phi_E$, the interaction term becomes nonnegligible, which occurs first for $\mu_E$ because $\phi_I < \phi_E$. Then, Eq. 4.35 is simplified to

$$\ln \phi_I + a_c (R_{g0}/d)^{5/3} = \ln \phi_E + a_\mu (\phi_E/\phi^*)^{5/4} \tag{4.36}$$

The right-hand side should be rather expressed by the virial expansion of $\mu$:

$$\ln \phi_I + a_c (R_{g0}/d)^{5/3} = \ln \phi_E + a_2 (\phi_E/\phi^*) \tag{4.37}$$

with $a_2/\phi^*$ being the second virial coefficient when the excess chemical potential is expanded with respect to $\phi$. The partition coefficient is then evaluated as

$$\boxed{\ln K = \ln K_0 + a_2 (\phi_E/\phi^*) \quad (\phi_E \ll \phi^*)} \tag{4.38}$$

The increase in $\phi_E$ results in an increase in $K$ because $a_2 > 0$ in the good solvent. The concentration increases more rapidly in the pore than it does in the surrounding solution. The positive second virial coefficient is the driving force to increase $K$.

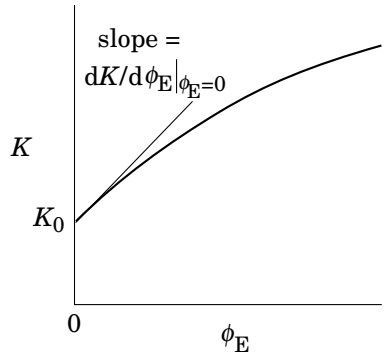


**Figure 4.23.** The tangential to the curve of $K$ at $\phi = 0$ has a positive slope in the good solvent.

The plot of $K$ versus $\phi$ has a positive slope at $\phi = 0$, as depicted in Figure 4.23. From Eq. 4.38, we find $dK/d\phi_E = a_2K/\phi^*$ at $\phi_E = 0$. Size exclusion chromatography (SEC) is based on the partitioning of a polymer chain with a small pore. Our naive expectation is that each polymer chain is partitioned between the pore and the surrounding solution independently of interactions of other chains. Equation 4.38 demonstrates, however, that the partition coefficient increases strongly with concentration. In terms of mass concentration $c_E$ in the exterior solution, Eq. 4.38 is written as

$$\ln K = \ln K_0 + 2A_2Mc_E \cong \ln K_0 + 4c_E/c^* \quad (c_E \ll c) \tag{4.39}$$

where $a_2\phi_E/\phi^*$ was replaced with $2A_2Mc_E$ (Problem 2.9), and $(16/9)A_2Mc = 3.49 \times c/c^*$ was used. For instance, if $K_0 = 0.1$ and $c^* = 5$ g/L, then $K \cong 0.22$ at $c/c^* = 1$ g/L. This is why an extremely low concentration is mandated for polymer solutions to be injected into the column in SEC. An overloading (injection of a solution more concentrated than $c^*/10$) significantly alters the chromatogram.

We can generalize the partitioning to solutions in solvents other than good solvents. With a decreasing $A_2$ (or $a_2$), the driving force weakens, and, when $A_2 = 0$, $dK/d\phi_E = 0$ at $\phi_E = 0$. The partition coefficient will remain unchanged over a wide range of concentrations before it starts to increase, helped by $A_3 > 0$. When $A_2 < 0$, $K$ will initially decrease, followed by an upturn at higher concentrations, as illustrated in Figure 4.24. Note that, in the low concentration limit, the chain with $A_2 > 0$ has the smallest $K_0$ because its dimension is the greatest.

***4.2.3.3 Partitioning at High Concentrations*** Now we consider the partitioning of the semidilute solution, $\phi_E/\phi^* > \phi_I/\phi^* \gg 1$. The entropy-of-mixing terms are now negligible compared with the other terms. Equation 4.35 is then simplified to

$$(\phi_I/\phi^*)^{5/4} + (a_c/a_\mu)(R_{g0}/d)^{5/3} = (\phi_E/\phi^*)^{5/4} \tag{4.40}$$

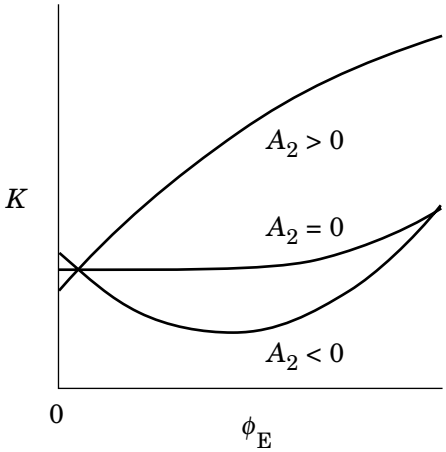


**Figure 4.24.** The concentration dependence of the partition coefficient $K$ is sensitive to the sign of the second virial coefficient $A_2$.

which leads to

$$K = [1 - (a_c/a_\mu)(R_{g0}/d)^{5/3}(\phi_E/\phi^*)^{-5/4}]^{4/5} \tag{4.41}$$

Recall that the correlation length $\xi$ is given by $\xi/R_{g0} \cong (\phi_E/\phi^*)^{-3/4}$ (Eq. 4.6). Then,

$$\boxed{\ln K \cong -(\xi/d)^{5/3} \quad (\phi_E \gg \phi^*)} \tag{4.42}$$

With an increasing $\phi_E$, $\xi$ decreases, and $K$ approaches unity.

Comparison of Eqs. 2.142 and 4.42 demonstrates that the partitioning of the semidilute solution is determined by the ratio of the correlation length $\xi$ (blob size) to the pore size in the same way as the partitioning of the dilute solution is governed by the ratio of the chain dimension $R_{g0}$ to the pore size. Figure 4.25 illustrates the partitioning in two concentration regimes. We expect a smooth change from $R_{g0}$ to $\xi$ as the concentration increases.

Because $\xi$ becomes progressively smaller with an increasing concentration, even long polymer chains, strongly excluded at low concentrations, can fill up the pore space at high concentrations. The limiting scenario is polymer melt. It will fill the pore space unless the pore surface is strongly repulsive, although it may take a long time. Eventually $K$ will approach unity. The crossover behavior is called a **weak-to-strong penetration transition**.[44] The transition occurs at around $\phi^*$, but a longer chain that has a smaller $K_0$ requires a higher concentration (Fig. 4.26).

### 4.2.4 PROBLEMS

**Problem 4.1:** The sequence of blobs that enclose monomers of a given polymer chain has a contour length $L_b \cong \xi N/g_N$. How does $L_b$ depend on $\rho/\rho^*$? Also

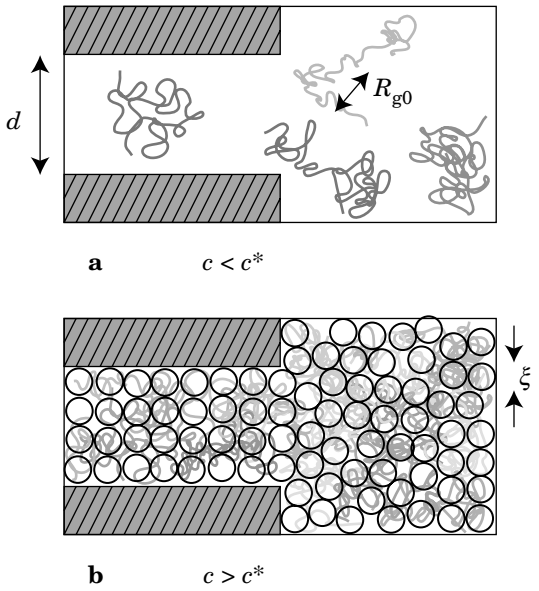


**Figure 4.25.** a: Partitioning of a dilute polymer solution is governed by the ratio of $R_{g0}$ to the pore diameter $d$. b: Partitioning of a semidilute polymer solution is governed by $\xi/d$.

show that $L_b < Nb$, where $Nb$ is the contour length of the polymer chain. Use $\nu = 3/5$.

**Solution 4.1:**

$$L_b \cong \xi(N/g_N) \cong R_{g0}(\rho/\rho^*)^{-3/4}(\rho/\rho^*)^{5/4} = R_{g0}(\rho/\rho^*)^{1/2}$$

$$\frac{L_b}{Nb} \cong \frac{(bN^{3/5})\rho^{1/2}\,(b^{3/2}N^{2/5})}{Nb} = (b^3\rho)^{1/2} < 1$$

because the concentration is still low, that is, $b^3\rho \ll 1$.

**Problem 4.2:** Show that

$$\frac{M}{N_A k_B T}\frac{\partial \Pi}{\partial c} = f_\Pi(x) + x f'_\Pi(x)$$

where $x = c/c^*$.

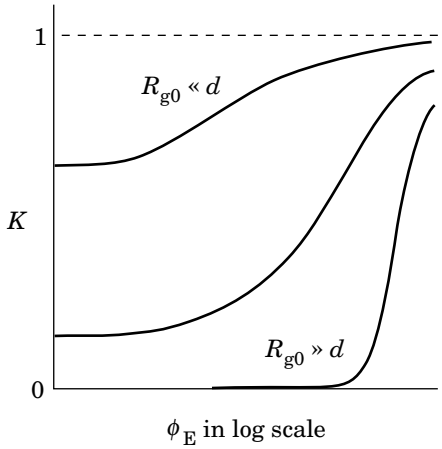


**Figure 4.26.** Weak-to-strong penetration transition. The partition coefficient $K$ is plotted as a function of the volume fraction of the polymer in the exterior solution. The transition requires a higher concentration with an increasing chain length.

**Solution 4.2:**

$$\frac{M}{N_A k_B T}\frac{\partial \Pi}{\partial c} = \frac{\partial}{\partial c}\left(c\frac{M\Pi}{cN_A k_B T}\right) = \frac{M\Pi}{cN_A k_B T} + c\frac{\partial}{\partial c}\frac{M\Pi}{cN_A k_B T}$$
$$= f_\Pi(x) + x\frac{\mathrm{d}}{\mathrm{d}x}f_\Pi(x)$$

**Problem 4.3:** Verify that Eq. 4.27 gives $A = N$ in the dilute solution limit as required.

**Solution 4.3:** At low concentrations, $\partial\Pi/\partial c = N_A k_B T/M$. Then, $A = N(N_A k_B T/M)\partial c/\partial\Pi = N$.

**Problem 4.4:** In the lattice chain model, the osmotic pressure is given as (Problem 2.4)

$$\Pi = \frac{\phi^2}{v_{site}}\frac{\partial}{\partial\phi}\frac{1}{\phi}\frac{\Delta A_{mix}}{n_{site}}$$

Use Eq. 2.26 to show that

$$\frac{\Delta\mu_{rep}(\phi)}{k_B T} = \ln(\phi) + P(\phi) - 1 + \int_0^\phi x^{-1}[P(x) - 1]\,\mathrm{d}x$$

where $P(\phi) \equiv \Pi(\phi)/\Pi_{ideal}(\phi)$.

**Solution 4.4:** From the given expression for $\Pi/k_BT$,

$$\frac{\Delta A_{\text{mix}}}{n_{\text{site}}} = v_{\text{site}}\phi\int\frac{\Pi}{\phi^2}\,\mathrm{d}\phi$$

Then, with Eq. 2.26,

$$\frac{\Delta\mu_{\text{rep}}(\phi)}{k_BT} = \frac{N}{n_{\text{site}}}\frac{\partial}{\partial\phi}\frac{\phi n_{\text{site}}v_{\text{site}}}{k_BT}\int\frac{\Pi}{\phi^2}\,\mathrm{d}\phi = \frac{\partial}{\partial\phi}\phi\int\frac{1}{\phi}\frac{\Pi}{\Pi_{\text{ideal}}}\,\mathrm{d}\phi$$
$$= \frac{\partial}{\partial\phi}\,\phi\int\frac{1}{\phi}P(\phi)\,\mathrm{d}\phi = \ln\phi + P(\phi) + \int\frac{P(\phi)-1}{\phi}\,\mathrm{d}\phi$$

We add a constant $-1$ to make the nonideal part of $\Delta\mu_{\text{rep}}$ disappear at $\phi = 0$:

$$\frac{\Delta\mu_{\text{rep}}(\phi)}{k_BT} = \ln\phi + P(\phi) - 1 + \int\frac{P(\phi)-1}{\phi}\,\mathrm{d}\phi$$

**Problem 4.5:** Show that $\delta\mu(c)/k_BT$ given by Eq. 4.28 is a function of $c/c^*$.

**Solution 4.5:** Let $\Pi(c)/\Pi_{\text{ideal}}(c) \equiv P(c/c^*)$. Then, the integral $I$ in Eq. 4.28 is expressed as

$$I \equiv \int_0^c x^{-1}[\Pi(x)/\Pi_{\text{ideal}}(x) - 1]\,\mathrm{d}x = \int_0^c x^{-1}[P(x/x^*) - 1]\,\mathrm{d}x$$

We change the variable of integration to $y \equiv x/c^*$. Then,

$$I = \int_0^{c/c^*}[P(y) - 1]\frac{\mathrm{d}y}{y}$$

Thus,

$$\frac{\delta\mu(c)}{k_BT} = P(c/c^*) - 1 + \int_0^{c/c^*}[P(y) - 1]\frac{\mathrm{d}y}{y}$$

**Problem 4.6:** Draw a sketch for the excess light scattering intensity $I_{\text{ex}}$ of a polymer solution in the theta solvent as a function of concentration $c$ of the polymer in a double logarithmic plot. Indicate the slope of the plot at each of $c/c^* \ll 1$ and $c/c^* \gg 1$.

**Solution 4.6:** At low concentrations, $I_{ex} \sim c$. At $c/c^* \gg 1$, $\partial\Pi/\partial c \sim c^2$ in the theta solvent. Then, $I_{ex} \sim c^{-1}$. The sketch is given below.

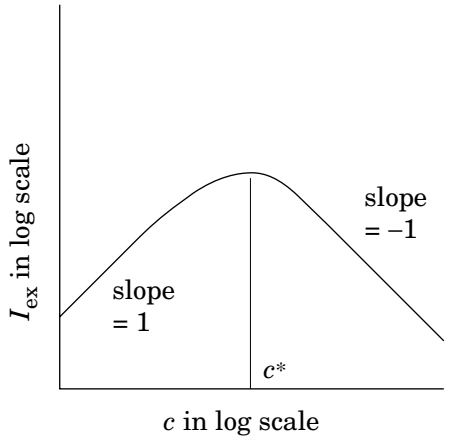


**Problem 4.7:** We can apply Flory's method to evaluate the chain contraction in the semidilute solution. In Flory's expression for the free energy of a polymer chain $A_{ch}$ in Eq. 1.63, the binary monomer–monomer interaction was limited to a pair on the same polymer chain. In the semidilute solution of monomer density $\rho$, the partner of the interaction is mostly the monomers on the other chains. We can approximate this change by introducing the probability $(N/R^3)/(N/R^3 + \rho)$. A monomer on a given polymer chain interacts with other monomers on the same chain with this probability. Then, Eq. 1.63 is changed to

$$\frac{A_{ch}}{k_B T} \cong \frac{R^2}{Nb^2} + b^3 \frac{N^2}{R^3} \frac{N/R^3}{N/R^3 + \rho}$$

In the semidilute solution, this equation is simplified to

$$\frac{A_{ch}}{k_B T} \cong \frac{R^2}{Nb^2} + b^3 \frac{N^3}{R^6} \frac{1}{\rho}$$

Show that minimization of $A_{ch}$ leads to the same contraction factor as the one predicted in the scaling theory.

**Solution 4.7:** From $(\partial/\partial R)(A_{ch}/k_B T) = 0$,

$$\frac{2R}{Nb^2} - 6b^3 \frac{N^3}{R^7} \frac{1}{\rho} \cong 0$$

which is rewritten to

$$R \cong b^{5/8} N^{1/2} \rho^{-1/8}$$

**Problem 4.8:** Compare the osmotic compressibility of a given polymer in the good solvent and in the theta solvent by drawing a sketch of $\Pi/\Pi_{\text{ideal}}$ as a function of $b^3\rho$ in a double logarithmic scale.

**Solution 4.8:**

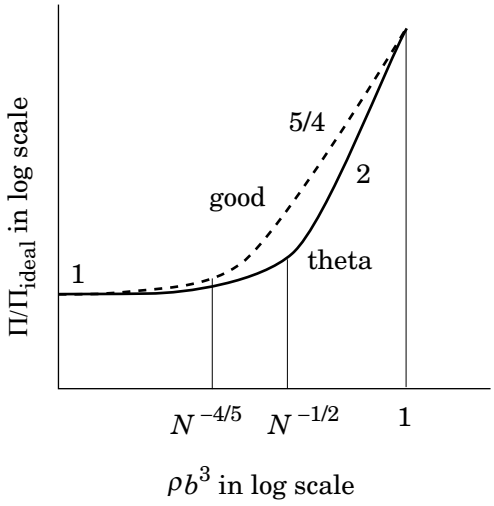


**Problem 4.9:** Estimate the effect of the chain contraction on the partition coefficient of the semidilute solution with a pore of diameter $d$.

**Solution 4.9:** When we allow $R_g$ to change with concentration,

$$\ln K \cong -(a_c/a_\mu)(R_g/d)^{5/3}(\phi_E/\phi^*)^{-5/4}$$

With $R_g/d$ given by

$$R_g/d = (R_g/R_{g0})(R_{g0}/d) \cong (\phi_E/\phi^*)^{-1/8}(R_{g0}/d)$$

we have

$$\begin{aligned}\ln K &\cong -[(R_{g0}/d)(\phi_E/\phi^*)^{-1/8}]^{5/3}(\phi_E/\phi^*)^{-5/4} \\ &= -(R_{g0}/d)^{5/3}(\phi_E/\phi^*)^{-35/24}\end{aligned}$$

The exponent is $-35/24 \cong -1.46$, as opposed to $-5/4 \cong -1.25$ in Eq. 4.41.

**Problem 4.10:** Discuss the partitioning of polymer chains in semidilute solution in the theta condition with a pore of diameter $d$. Can the partitioning of the semidilute solution be treated as the partitioning of independent blobs?

**Solution 4.10:** In the theta condition, Eq. 4.40 is rewritten to

$$(\phi_I/\phi^*)^2 + (a_c/a_\mu)(R_{g0}/d)^2 = (\phi_E/\phi^*)^2$$

which leads to

$$\ln K = -(a_c/a_\mu)(R_{g0}/d)^2(\phi_E/\phi^*)^{-2}$$

Because $\xi/R_{g0} \cong (\phi_E/\phi^*)^{-1}$,

$$\ln K \cong -(\xi/d)^2$$

This equation demonstrates that the partitioning of the semidilute solution is equivalent to the partitioning of independent blobs in the theta condition. Compare the last equation with Eq. 2.136.

## 4.3 DYNAMICS OF SEMIDILUTE SOLUTIONS

### 4.3.1 Cooperative Diffusion

In Section 3.2, we learned that dynamic light scattering (DLS) measures the mutual diffusion coefficient $D_m$ and that it increases with an increasing polymer concentration in the good solvent. We extend it here to the semidilute solution. Figure 4.27

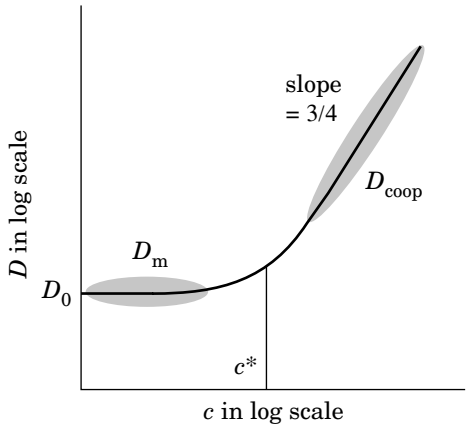


**Figure 4.27.** Diffusion coefficient measured in DLS for various concentrations of a polymer in a good solvent is schematically shown as a function of polymer concentration $c$. In the low concentration limit, it is $D_0$, the diffusion coefficient of an isolated chain. With an increasing concentration, the mutual diffusion coefficient $D_m$ increases linearly, followed by a sharp upturn to a crossover to the cooperative diffusion coefficient $D_{coop}$ in the semidilute solution. The latter increases in a power law with an exponent close to $3/4$.

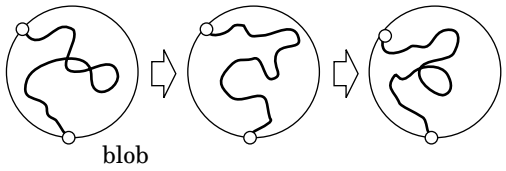


**Figure 4.28.** Monomer density fluctuation within a blob. The monomers can rearrange internally without changing the connection to the outside world.

shows schematically how the diffusion coefficient measured in DLS changes with the polymer concentration $c$ in a wide range of concentrations.

The diffusion coefficient $D_0$ in the dilute solution limit gives the hydrodynamic radius $R_H$ of the isolated polymer chain in solution. The mutual diffusion coefficient $D_m$ increases linearly with concentration in the dilute regime, $c \ll c^*$, as we have seen in Section 3.2.11. The increase is mostly ascribed to repulsive interactions between polymer chains that are manifested in the positive second virial coefficient. With a further increase in $c$, $D_m$ deviates upward from the linear relationship. As $c$ exceeds $c^*$ and the solution enters the semidilute regime, the diffusion coefficient starts to follow a straight line in a double logarithmic scale. The mutual diffusion observed by DLS in the semidilute solution is called the **cooperative diffusion**, since it represents cooperative motion of monomers within a blob. As Figure 4.28 illustrates, the partial chain within a blob is constantly rearranging itself without a need to move the two anchoring points. The dynamics follows a diffusion equation. As we will find below, the **cooperative diffusion coefficient** ($D_{coop}$) is related to the blob size $\xi$ (=correlation length) by

$$\boxed{D_{coop} = \frac{k_B T}{6\pi\eta_s \xi} \qquad \text{cooperative diffusion coefficient}} \tag{4.43}$$

As $\xi$ decreases with an increasing concentration, the cooperative diffusion becomes faster. Because $\xi \sim c^{-\nu/(3\nu - 1)}$, $D_{coop}$ increases as $D_{coop} \sim \xi^{-1} \sim c^{\nu/(3\nu - 1)}$. In the good solvent, $D_{coop} \sim c^{3/4}$. In the theta solvent, $D_{coop} \sim c$. These dependences are included in Table 4.1. Note that $D_{coop}$ is independent of the molecular weight of the polymer.

We can use Eq. 4.43 to estimate the correlation length $\xi$ of a given semidilute solution from the measurement of $D_{coop}$ in DLS. The correlation length estimated in this way is often called the **dynamic correlation length**. Figure 4.29 shows an example for semidilute solutions of polystyrene with different molecular weights in various good solvents.[51] The data are on a straight line with a slope close to $-3/4$.

The difference in the expression of the diffusion coefficient between the single-chain diffusion (Eq. 3.54) and the cooperative diffusion is only $R_H$ and $\xi$. The motional unit of size $R_H$ gives way to the blob size $\xi$ as the concentration exceeds $c^*$.

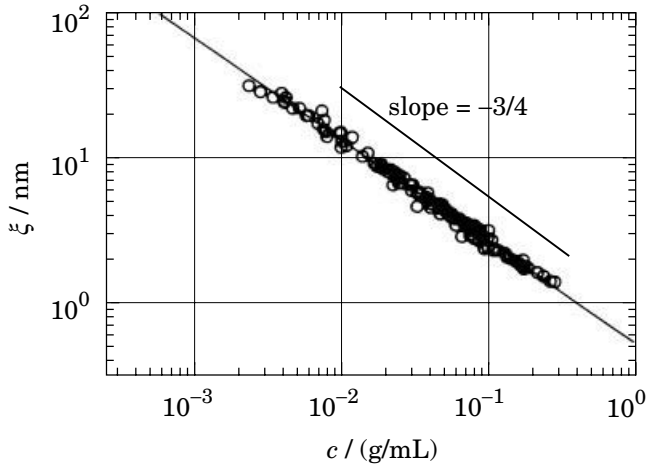


**Figure 4.29.** Correlation length $\xi$ estimated from the cooperative diffusion coefficient. Data were obtained for polystyrene of different molecular weights in various good solvents. (From Ref. 51.)

The reason why $D_{\text{coop}}$ is given by Eq. 4.43 is as follows. In Section 3.2.7, we learned that the hydrodynamic radius $R_{\text{H}}$ of a linear chain polymer is given as the reciprocal of the average of $r^{-1}$, where $r$ is the distance between two monomers on the chain. We used the definition to estimate $R_{\text{H}}$ for a chain with a Gaussian chain conformation. We can use the same formula to calculate $D_{\text{coop}}$ for the cooperative dynamic mode of the blob. It is given by

$$D_{\text{coop}} = \frac{k_{\text{B}}T}{6\pi\eta_{\text{s}}}\left\langle\frac{1}{r}\right\rangle \tag{4.44}$$

where $r$ is the distance between two monomers that move cooperatively. The distance $r$ is distributed with the Ornstein–Zernike correlation function. From Eq. 4.24,

$$\left\langle\frac{1}{r}\right\rangle = \frac{\displaystyle\int_0^\infty 4\pi r^2 \frac{1}{r} g_{\text{OZ}}(r)\,\mathrm{d}r}{\displaystyle\int_0^\infty 4\pi r^2 g_{\text{OZ}}(r)\,\mathrm{d}r} = \frac{1}{\xi} \tag{4.45}$$

Thus we obtain Eq. 4.43.

The decay rate $\Gamma$ in the autocorrelation function $|g_1(\tau)|$ for this cooperative mode is proportional to $\mathbf{k}^2$. It means that the monomer density fluctuation within the blob is diffusional. There is a good reason for this dynamic mode to be called the cooperative diffusion.

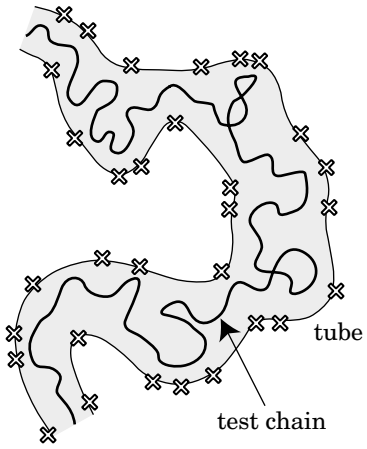


**Figure 4.30.** The test chain is trapped in a tube (indicated by the gray area) created by neighboring chains. The crossings represent the intersection of the neighboring chains with the curved surface on which the test chain lies.

### 4.3.2 Tube Model and Reptation Theory

***4.3.2.1 Tube and Primitive Chain*** In the preceding subsection, we paid attention to the short-time motion of monomers within a blob. The motion does not involve translation of the polymer chain as a whole. Here we look at the overall motion of the chain over a distance longer than the blob size.

Polymer melts and semidilute and concentrated solutions of polymer are highly viscous. Even at a concentration of 1 wt %, solutions of polymer with a molecular weight greater than several million g/mol can flow only slowly. Their behaviors are even elastic like rubber at accessible time and frequency ranges. These exquisite properties had eluded researchers for decades until the **tube model** and the **reptation theory** elegantly solved the mystery. The tube model and the reptation theory were introduced by de Gennes.[44] They were refined and applied to the viscoelasticity of semidilute solutions of polymers and polymer melts in the late 1970s by Doi and Edwards.[45] Until then, there had been no molecular theory to explain these phenomena. We will learn the tube model and the reptation theory here.

We pick up a single chain, called a **test chain**, out of many chains in the solution. The test chain is highly entangled with neighboring chains. We can imagine a **tube**-like region surrounded by these neighboring chains around the test chain, as illustrated in Figure 4.30. These neighboring chains prohibit the test chain from moving beyond them, effectively confining the test chain into a tubelike region. Although the contour of the test chain is winding in three dimensions, we draw a two-dimensional illustration in which the test chain is constrained to the tube, as shown in the figure. We can regard the illustration as being drawn on the surface, curved along the test chain's contour and then pulled flat. The crosses in the figure represent intersections of the neighboring chains with the surface. Within the tube,

the test chain is winding. The tube diameter varies along the test tube's contour and also in time.

The tube model assumes the followings:

(1) Over a short period of time, the test chain wiggles within the tube just as the monomers in the blob move cooperatively without moving out of the blob (Section 4.3.1).
(2) Beyond that time scale, the test chain can move only along the tube. The test chain cannot move beyond the constraints imposed by the tube.
(3) The head portion of the test chain can explore the next direction freely. As the head moves out of the existing tube, a new section is added to the tube. At the same time, the tail vacates a portion of the existing tube. Overall, there is little change in the length of the tube with time.

Later we will find that the test chain that follows the above assumptions makes a diffusional motion in the solution at sufficiently long times, although it is slow. The freedom allowed for the ends of the test chain makes the diffusion possible.

We learned in Section 4.2.2 that the polymer chain in the semidilute solution takes a conformation of an ideal chain. We therefore can use a random-walk model to construct the test chain. Let the random walk consist of $N$ independent steps of step length $b$. Then, the contour length of the test chain is $Nb$, and the mean square end-to-end distance is $Nb^2$.

It is convenient to define a **primitive chain**. It is the centerline of the tube. The test chain wiggles around the primitive chain (Fig. 4.31). The motion of the primitive chain is nothing more than a coarse-grained view for the motion of the test chain it represents. Wiggling motion in the short time scale is averaged to form the primitive chain.

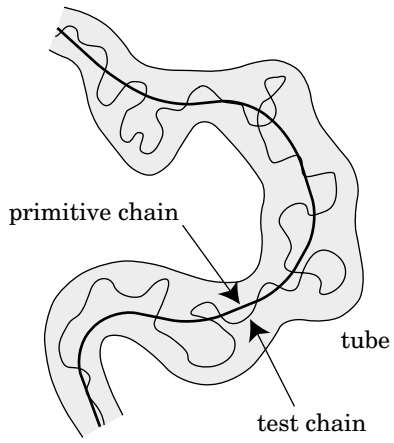


**Figure 4.31.** The primitive chain lies along the centerline of the tube. The test chain winds around the primitive chain.

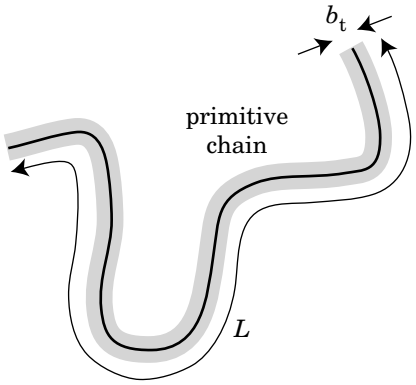


**Figure 4.32.** The primitive chain is regarded as an ideal chain of a step length of $b_t$ and a contour length of $L$. The primitive chain and the test chain share the end-to-end distance.

According to the three assumptions of the tube model given earlier, the primitive chain moves only along its contour. Its motion is like a snake slithering on earth. This motion is called **reptation**. The end of the primitive chain can explore its next direction, but the rest follows its own existing path.

The primitive chain shares some of the statistical properties with the parent test chain. Both are ideal. Their end-to-end distance is the same. The conformation of the primitive chain is a coarse-grained version of the conformation of the test chain. When we apply the random-walk model to the primitive chain, its step length is equal to the tube diameter $b_t$ (Fig. 4.32). Because the tube encases the test chain, $b_t > b$. We can appreciate the coarse-grained nature of the primitive chain in this inequality. The contour length $L$ of the primitive chain is shorter than that of the test chain. We can estimate $L$ as follows. For the primitive chain to have a contour length of $L$, the random walk must have $L/b_t$ steps. We equate the mean square end-to-end distance of the test chain and that of the primitive chain: $b_t^2(L/b_t) \cong b^2N$. Then,

$$L \cong b^2N/b_t \tag{4.46}$$

For now, we proceed without knowing how to assess $b_t$. Just as the blob size, $b_t$ will depend on the monomer density but not on the chain length; the density of crosses in Figure 4.30 is determined by the monomer density not by the chain length. Later, we will find the dependence.

***4.3.2.2 Tube Renewal*** We illustrate in Figure 4.33 how the primitive chain changes its shape by continuously renewing its head or tail. The tube moves together with the primitive chain.

The primitive chain in panel a slides along its own contour. The advancing end emerges from the existing tube and finds a new path, just as a random walker moves another step forward, as shown in panel b. A new section is added

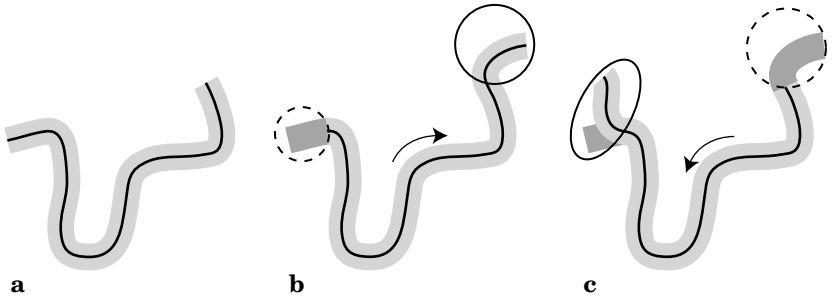


**Figure 4.33.** The tube changes its shape and position when the primitive chain slides along its contour. When the primitive chain moves from the one shown in panel a to the one shown in panel b, the advancing end adds a new portion to the existing tube (shown as a solid circle) and the receding end discards the other end of the old tube (shown as a dashed circle). When the primitive chain reverses its direction (panel c), the advancing end does not need to go back into the old tube. A new section is added at the advancing end, and an old section is depleted from the other end.

immediately to the growing end of the tube. At the same time, the receding end of the primitive chain vacates a portion of the existing tube, effectively annihilating the end of the tube. When the primitive chain reverses its course and goes back along its contour, as shown in panel c, the advancing end, formerly the receding end, does not need to move back into the old tube. The new advancing end can freely choose another path. Thus, a new section is always added to the tube while the other end is destroyed. The motion of the primitive chain is made possible by the motion of the test chain. As the test chain moves out of the existing tube while wiggling around, the new section of the tube is created. Along with the creation and annihilation of the tube sections, the primitive chain itself grows at one end and declines at the other end.

As the primitive chain moves back and forth along its own contour, the chain constantly renews the end portions of the tube. In each reversal of the course, the primitive chain adds a new section and loses a part of the memory regarding the constraint it had earlier. In Figure 4.34, panel a depicts the tube and the primitive chain when they have still some memory of the old tube. Eventually, none of the trace will be left of the old tube, as shown in panel b. The complete renewal can occur even when the centroid of the primitive chain is at the same position as the one when we started tracking the motion of the primitive chain. More likely, though, the primitive chain moves over a distance of its end-to-end distance. So does the test chain. In other words, the tube renewal occurs each time the centroid of the primitive chain moves the distance of $bN^{1/2}$.

***4.3.2.3 Disengagement*** The tube renewal is made possible by reptation of the primitive chain along its own contour. To estimate the time necessary for the tube renewal, we need to know the nature of the reptation motion. The motion is a one-dimensional diffusion along a curve in three dimensions. Whether the primitive

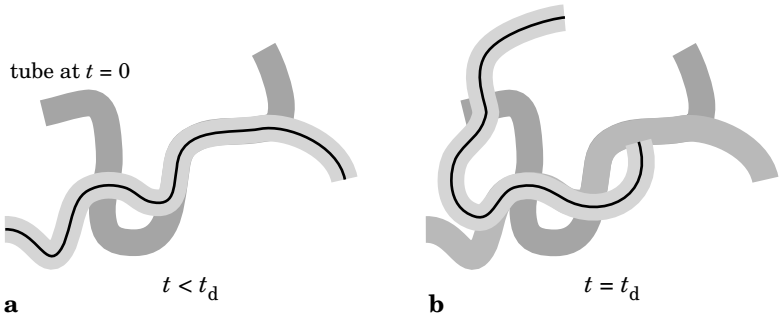


**Figure 4.34.** Tube renewal. a: The tube at a certain time (light gray) shares a part with the old tube that enclosed the test chain at $t = 0$ (dark gray). b: The tube renewal continues, and finally the tube (light gray) shares no part with the old tube. The time needed to reach the latter state is called the disengagement time ($t_d$).

chain moves back or forth is stochastic, reflecting the random motion of the test chain.

In the semidilute solution, the hydrodynamic interactions are shielded over the distance beyond the correlation length, just as the excluded volume is shielded. We can therefore approximate the dynamics of the test chain by a Rouse model, although the motion is constrained to the space within the tube. In the Rouse model, the chain as a whole receives the friction of $N\zeta$, where $\zeta$ is the friction coefficient per bead. When the motion is limited to the curvilinear path of the primitive chain, the friction is the same. Because the test chain makes a Rouse motion within the tube, only the motion along the tube survives over time, leading to the translation of the primitive chain along its own contour. The one-dimensional diffusion coefficient $D_c$ for the motion of the primitive chain is called the **curvilinear diffusion coefficient**. It is therefore equal to $D_G$ of the Rouse chain (Eq. 3.160) and given by

$$D_c \cong \frac{k_B T}{N\zeta} \tag{4.47}$$

When the primitive chain slides along the tube with $D_c$, the **disengagement time** $t_d$, the time needed for the primitive chain to renew its encasing tube, is given as

$$t_d \cong \frac{L^2}{D_c} \tag{4.48}$$

In $t_d$, the primitive chain escapes the existing tube. With Eqs. 4.46 and 4.47, $t_d$ is rewritten to

$$\boxed{t_d \cong \frac{b^4 N^3 \zeta}{{b_t}^2 k_B T} \qquad \text{disengagement time}} \tag{4.49}$$

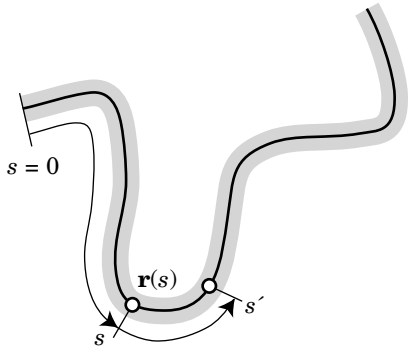


**Figure 4.35.** Two points, $s$ and $s'$, on the primitive chain. Their mean square distance in the three-dimensional space is $b_t|s - s'|$.

The disengagement time is proportional to $N^3$. A slight increase in $N$ leads to a large increase in $t_d$. The overall dynamics of the chains becomes a lot slower.

Let us compare $t_d$ and $\tau_1$, the relaxation time of the first normal mode of the Rouse chain in the absence of entanglement. With $\tau_1 \cong \zeta N^2 b^2/k_B T$ (Eq. 3.136), we obtain

$$t_d/\tau_1 \cong Nb^2/{b_t}^2 \cong L/b_t \tag{4.50}$$

which is equal to the number of steps for the primitive chain in the random walk model. The chain is sufficiently long, and therefore $L/b_t \gg 1$. Thus, $t_d \gg \tau_1$.

***4.3.2.4 Center-of-Mass Motion of the Primitive Chain*** First, we consider the motion of a point on the primitive chain when it makes one-dimensional diffusion. In Figure 4.35, we represent the contour of the primitive chain at a given time by $\mathbf{r}(s)$, where $s$ is the distance along the chain measured from one of the chain ends, as we did for the wormlike chain in Section 1.5. Because $\mathbf{r}(s)$ is described by the ideal chain model, the mean square distance measured in the three-dimensional space between two points $s$ and $s'$ on the primitive chain is given by (step length)$^2$ $\times$ (number of steps). The step length is $b_t$. The contour between $s$ and $s'$ that registers the curvilinear length of $|s - s'|$ has $|s - s'|/b_t$ steps. Thus,

$$\langle [\mathbf{r}(s) - \mathbf{r}(s')]^2 \rangle \cong b_t|s - s'| \tag{4.51}$$

Now we move the primitive chain. The chain reptates along the tube with a diffusion coefficient $D_c$. The point at $s = s(0)$ moves with the same diffusion coefficient $D_c$. We record the slithering motion of the point by the curvilinear distance measured from the end of the primitive chain at $t = 0$ (gray line), as shown in Figure 4.36. Let the point on the primitive chain slide to $s(t)$ in time $t$. Then, the one-dimensional displacement $s(t) - s(0)$ along the contour of the primitive chain

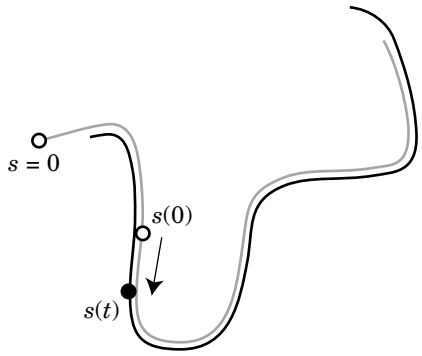


**Figure 4.36.** The primitive chain slides along its own contour. The point $s(0)$ moves to $s(t)$, but it is still on the contour of the chain at $t = 0$, drawn in light gray. The distance $s$ is measured from the end of the primitive chain at $t = 0$.

is given as

$$[s(t)-s(0)]^2 \cong D_c t \tag{4.52}$$

When $t < t_d$, most of the points on the primitive chain stay on its contour at $t = 0$. The two points $s$ and $s'$ in Eq. 4.51 can be $s(0)$ and $s(t)$, respectively. Thus,

$$\langle [\mathbf{r}(s(t)) - \mathbf{r}(s(0))]^2 \rangle \cong b_t |s(t)-s(0)| \cong b_t (D_c t)^{1/2} \tag{4.53}$$

The mean square displacement in the three-dimensional space for a point on the primitive chain is proportional to $t^{1/2}$. Figure 4.37 illustrates the difference between the two distances. Recall that the mean square displacement is proportional to $t$ in regular, unrestricted diffusion in solution. The exponent $1/2$ in Eq. 4.53 is due to the one-dimensional random walk on a path created by another random walker in the three-dimensional space.

The $t^{1/2}$ dependence is limited to $t < t_d$. As the primitive chain escapes the presently trapping tube in $t_d$, it may change the dependence in the time scale of $t > t_d$. Now we pay attention to the overall movement of the primitive chain in that time scale. The overall movement consists of step motions. In each step time, the end of the primitive chain moves a distance of $b_t$ to find a new direction. The rest of the chain follows the existing contour. The step time $t_1$ is the time needed for the one-dimensional diffusion to move a distance of $b_t$ with the diffusion coefficient $D_c$, that is, $D_c t_1 \cong b_t^2$. Thus,

$$t_1 \cong b_t^{\,2}/D_c \tag{4.54}$$

The step displacement for the centroid of the primitive chain in time $t_1$ is evaluated as follows. The contour of the primitive chain at $t = 0$ is given as $\{\mathbf{r}(s); 0 \le s \le L\}$. The contour at $t = t_1$ is built on the contour at $t = 0$. We can use the contour

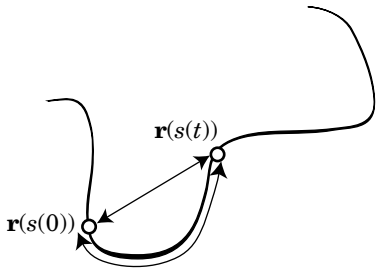


**Figure 4.37.** The mean square distance between $\mathbf{r}(s(t))$ and $\mathbf{r}(s(0))$ in the three-dimensional space is around $(D_c t)^{1/2}$. The mean square distance between the two points measured along the contour of the primitive chain is around $D_c t$.

$\mathbf{r}(s)$ at $t = 0$ to describe the contour at $t = t_1$ as $\{\mathbf{r}(s);\, b_t \le s \le L + b_t\}$. In the latter, $\{\mathbf{r}(s);\, L \le s \le L + b_t\}$ represents the newly created portion and $\{\mathbf{r}(s);\, 0 \le s \le b_t\}$ is the discarded portion. The rest is the same as the contour at $t = 0$ (Fig. 4.38). The center-of-mass positions $\mathbf{r}_G(0)$ and $\mathbf{r}_G(t_1)$ of the primitive chain at $t = 0$ and $t = t_1$ are respectively given as

$$\mathbf{r}_G(0) = L^{-1}\int_0^L \mathbf{r}(s)\,ds, \qquad \mathbf{r}_G(t_1) = L^{-1}\int_{b_t}^{L+b_t} \mathbf{r}(s)\,ds \tag{4.55}$$

Then,

$$\mathbf{r}_G(t_1) - \mathbf{r}_G(0) = L^{-1}\int_0^{b_t} [\mathbf{r}(L + s) - \mathbf{r}(s)]\,ds \tag{4.56}$$

Its mean square is

$$\langle [\mathbf{r}_G(t_1) - \mathbf{r}_G(0)]^2 \rangle = L^{-2}\int_0^{b_t}\int_0^{b_t} \langle [\mathbf{r}(L + s) - \mathbf{r}(s)] \cdot [\mathbf{r}(L + s') - \mathbf{r}(s')] \rangle\, ds\, ds' \tag{4.57}$$

Because $b_t \ll L$, $\mathbf{r}(L + \mathbf{s}) - \mathbf{r}(s) \cong \mathbf{r}(L) - r(0)$ for $0 < s < b_t$. Thus, the mean square displacement in one step is

$$\begin{aligned} \langle [\mathbf{r}_G(t_1) - \mathbf{r}_G(0)]^2 \rangle &\cong L^{-2}\int_0^{b_t}\int_0^{b_t} \langle [\mathbf{r}(L) - \mathbf{r}(0)]^2 \rangle\, ds\, ds' \\ &\cong L^{-2}\int_0^{b_t}\int_0^{b_t} Nb^2\, ds\, ds' = Nb^2 {b_t}^2/L^2 \end{aligned} \tag{4.58}$$

The primitive chain repeats this step motion to move its center of mass. Each step is independent because the chain end is free to choose its next direction. The displacement in the second step, $\mathbf{r}_G(2t_1) - \mathbf{r}_G(t_1)$, is uncorrelated with the displacement

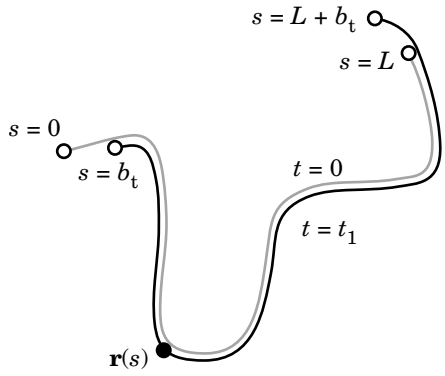


**Figure 4.38.** The primitive chain at $t = t_1$ is on the contour of the chain at $t = 0$ and its extension. The chain at $t_1$ occupies the portion from $s = b_t$ to $s = L + b_t$ measured from one end of the primitive chain at $t = 0$.

in the first step, $\mathbf{r}_G(t_1) - \mathbf{r}_G(0)$. Thus, the ratio of the mean square displacement to the step time gives the center-of-mass diffusion coefficient $D_G$ of the primitive chain in solution:

$$D_G \cong \frac{\langle [\mathbf{r}_G(t_1) - \mathbf{r}_G(0)]^2 \rangle}{t_1} \cong \frac{Nb^2 {b_t}^2}{L^2} \frac{D_c}{{b_t}^2} = D_c \frac{Nb^2}{L^2} \tag{4.59}$$

With Eqs. 4.46 and 4.47,

$$\boxed{D_G \cong \frac{k_B T {b_t}^2}{N^2 \zeta b^2} \quad \begin{array}{l}\text{diffusion coefficient} \\ \text{reptation theory}\end{array}} \tag{4.60}$$

Note that this $D_G$ is also the center-of-mass diffusion coefficient for the test chain. $D_G$ decreases as $\sim N^{-2}$ with an increasing chain length. The absolute value of the exponent is much greater compared with the center-of-mass diffusion coefficient of linear chain polymer in dilute solutions in which $D_G \sim N^{-1}$ for the Rouse chain and $\sim N^{-1/2}$ for the Zimm model in the theta condition.

How much does the primitive chain move its center of mass in $t_d$ with this diffusion coefficient? From Eqs. 4.49 and 4.60, it is easy to find that

$$D_G t_d \cong Nb^2 \tag{4.61}$$

As the primitive chain renews the existing tube, its center of mass moves a distance equal to its end-to-end distance, a reasonable result.

***4.3.2.5 Estimation of the Tube Diameter*** So far, we have been using the tube diameter $b_t$ as a given quantity. We expect that the tube will become thinner as the concentration increases and therefore the other chains impose crossings nearer to

the test chain. As $D_G \sim b_t^2$, we expect $D_G$ to decrease with an increasing concentration. To find the dependence, we simply apply the scaling theory to $D_G$ and assume

$$D_G = D_{G0} f_G(\rho R_{g0}^3/N) \tag{4.62}$$

where the scaling function $f_G(x)$ satisfies

$$f_G(x) \begin{cases} = 1 & (x \to 0) \\ \cong x^m & (x \gg 1) \end{cases} \tag{4.63}$$

with a scaling exponent $m$. Because $D_{G0} \cong k_B T/(\eta_s R_{g0})$, $D_G$ at $\rho R_{g0}^3/N \gg 1$ is

$$D_G = \frac{k_B T}{\eta_s R_{g0}} (\rho R_{g0}^3/N)^m \cong \frac{k_B T}{\eta_s} \rho^m b^{3m-1} N^{\nu(3m-1)-m} \tag{4.64}$$

where $R_{g0} \cong bN^\nu$ was used. The requirement that this $D_G$ have the same $N$ dependence as Eq. 4.60 leads to $\nu(3m - 1) - m = -2$; that is, $m = (\nu - 2)/(3\nu - 1)$. The exponent $m$ is $-7/4$ for $\nu = 3/5$. Thus, $D_G$ decreases with $c$ in the good solvent as

$$\boxed{D_G/D_{G0} \cong (c/c^*)^{-7/4} \qquad \text{good solvent}} \tag{4.65}$$

If we use $\nu = 0.59$, $m = -1.83$. In the theta solvent, $m = -3$. The decrease is steeper:

$$\boxed{D_G/D_{G0} \cong (c/c^*)^{-3} \qquad \text{theta solvent}} \tag{4.66}$$

The comparison of Eqs. 4.60 and 4.64 with $m = -7/4$ allows us to estimate $b_t$ for the good solvent condition. It is obtained as

$$b_t \cong (\zeta/\eta_s)^{1/2} b^{-17/8} \rho^{-7/8} \tag{4.67}$$

With an increasing $\rho$, $b_t$ decreases in a power with an exponent of $-7/8$. As required, $b_t$ is independent of $N$.

***4.3.2.6 Measurement of the Center-of-Mass Diffusion Coefficient*** The center-of-mass diffusion coefficient $D_G$ we obtained here is the self-diffusion coefficient $D_s$. DLS cannot measure the self-diffusion coefficient. It is necessary to use more specialized techniques such as FRS, FRAP, and PFG-NMR, described in Section 3.2.11. Figures 4.39 and 4.40 show examples of FRS studies of $D_s$ for dye-labeled polystyrene in benzene.[52]

Figures 4.39 shows a plot of $D_s$ as a function of the molecular weight $M$ of the polymer at two concentrations, 0.1 and 0.2 g/g (mass fraction of the polymer in solution), in the semidilute regime. The data at each concentration are apparently on a straight line with a slope of $-2$, in agreement with the prediction given by

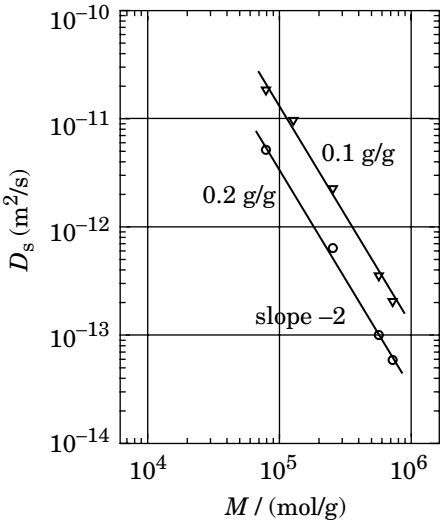


**Figure 4.39.** Self-diffusion coefficient $D_s$ of dye-labeled polystyrene in benzene at different concentrations, plotted as a function of the molecular weight $M$ of the polymer. The lines have a slope of $-2$. (From Ref. 52.)

Eq. 4.60. The concentration dependence of $D_s$ is shown in Figures 4.40. There is a gradual decrease in $D_s$ with an increasing concentration. The data obtained for the semidilute solutions are on straight lines with a slope of $-7/4$, in agreement with Eq. 4.65.

We can use DLS to measure the tracer diffusion coefficient $D_t$ in a ternary solution of two polymers and a solvent. The concentration of the matrix polymer is changed widely from dilute to semidilute, whereas the concentration of the probe polymer is held low. It is necessary to choose a solvent that is isorefractive with the matrix polymer and at the same time is nonselective to the two polymers. Then, DLS will selectively detect the light scattering from the probe polymer. For $D_t$ to simulate $D_G$, the interaction between the matrix polymer and probe polymer must be identical to the interaction between the matrix polymers. We hope that a pair of miscible polymers such as polystyrene probe and poly(vinyl methyl ether) matrix will satisfy this requirement. Figure 4.41 shows an example for the pair.[53] The common solvent is *o*-fluorotoluene. The figure shows a plot of $D_t$ as a function of $M_{PS}$, the molecular weight of polystyrene, for different concentrations of the matrix polymer (molecular weight $= 1.3 \times 10^6$ g/mol). In the absence of the matrix, $D_t \sim M_{PS}^{-0.56}$, indicating self-diffusion of isolated polystyrene chains in a good solvent. With an increasing matrix concentration, the slope becomes steeper. In the semidilute solutions, the slope is around $-2$, in agreement with Eq. 4.60 assuming $D_t \cong D_G$.

***4.3.2.7 Constraint Release*** The reptation theory assumes that the environment is frozen while the test chain moves. This assumption is questionable. The other

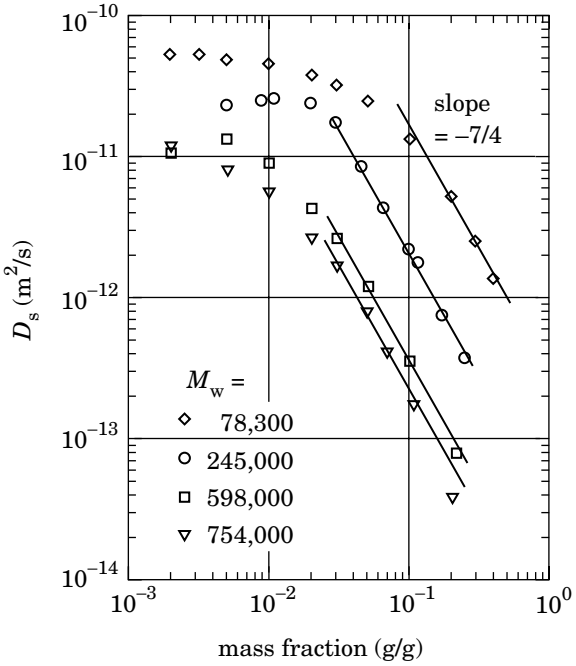


**Figure 4.40.** Self-diffusion coefficient $D_s$ of dye-labeled polystyrene of different molecular weights $M_w$ in benzene, plotted as a function of the polymer mass fraction. The lines have a slope of $-7/4$. (From Ref. 52.)

chains surrounding the test chain are moving in the same way in the same time scale as the test chain moves. Some entanglement points will come loose. New entanglement points will be created, as shown in Figure 4.30, while the test chain tries to get out of the existing tube. Annihilation and creation of the entanglement points will allow the tube to be renewed by another mechanism—**constraint release**. In the latter, the motion of the test chain is not limited to the one along the tube. The test chain can also move laterally.

***4.3.2.8 Diffusion of Polymer Chains in a Fixed Network*** Although the tube model and the reptation model were originally developed to explain the diffusion of polymer chains in concentrated solutions and melts, we can use it more naturally for the motion of polymer chains in a fixed network, for instance, a cross-linked network of polymer swollen in a good solvent. In the fixed network, the constraint release is absent. Therefore, we should be able to observe the reptation without being compromised.

The cross-linked network of polymer is called a **gel**. In the absence of the cross-linking, the swollen gel would form a solution. A probe polymer is added to the gel matrix, and the motion of the probe chains is traced by using DLS. The solvent needs to be isorefractive with the gel matrix to allow one to selectively detect the

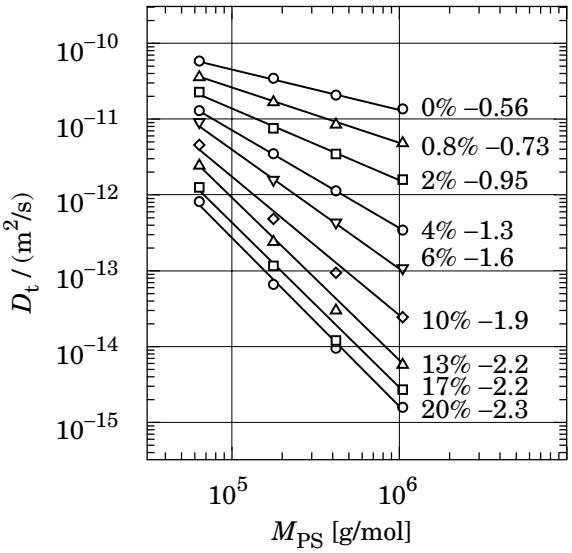


**Figure 4.41.** Tracer diffusion coefficient $D_t$ of polystyrene in solutions of matrix polymer, poly(vinyl methyl ether), in *o*-fluorotoluene at various concentrations of the matrix polymer, plotted as a function of molecular weight $M_{PS}$ of polystyrene. The solvent is isorefractive with the matrix polymer. The concentration of the matrix polymer and the slope obtained in the best fitting by a power law (straight line) are indicated adjacent to each plot. (From Ref. 53.)

scattering by the probe chains. Figure 4.42 shows an example for the tracer diffusion coefficient $D_t$ of the probe chains.[54] The matrix is cross-linked poly(vinyl methyl ether) swollen is toluene. The probe is linear polystyrene of different molecular weights. For sufficiently high molecular weights $M_{PS}$ of polystyrene, $D_t$ decreases in a power law of $M_{PS}^{-2.8}$, steeper than the theoretically predicted $M_{PS}^{-2}$. Other experimental techniques can also be used, for instance, FRS, FRAP, and PFG-NMR.

***4.3.2.9 Motion of the Monomers*** Here, we consider the mean square displacement of monomers on the entangled chains. Over a long time, $t > t_d$, the mean square displacement of the monomer, $\langle[\mathbf{r}_n(t) - \mathbf{r}_n(0)]^2\rangle$, becomes identical to the mean square displacement of the centroid of the primitive chain. Our interest is the short-time behavior in $t < t_d$. We expect that the monomers have a greater mobility in short time scales as in the bead-spring chain, which was discussed in Section 3.4.

We focus our attention primarily on the time range of $t > t_e$, where $t_e$ is the time for the mean square displacement of a monomer on the test chain to reach $b_t^2$. At $t < t_e$, the test chain wiggles within the tube without feeling the presence of the geometrical constraint imposed by neighboring chains. At $t > t_e$, the motion of the test chain is the same as that of the primitive chain.

In Sections 4.3.2.3 and 4.3.2.4, we assumed that the primitive chain follows a simple one-dimensional diffusion along its contour. This view is correct only for

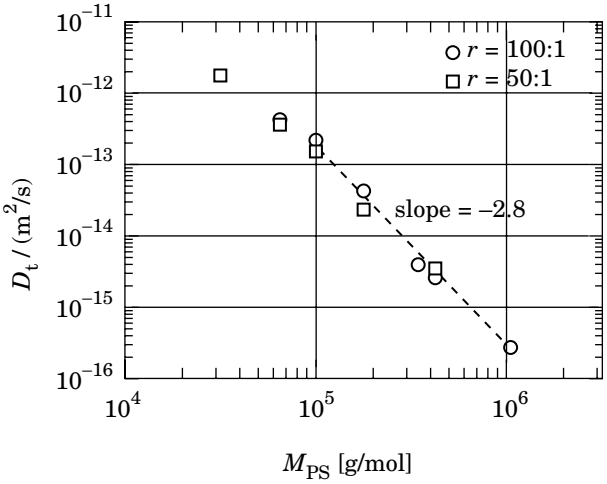


**Figure 4.42.** Tracer diffusion coefficient $D_t$ of polystyrene in a cross-linked matrix of poly(vinyl methyl ether) in toluene, plotted as a function of molecular weight $M_{PS}$ of polystyrene. The concentration of the matrix gel was 0.235 g/mL. The monomer to cross-linker ratio, $r$, was 100 and 50. The dashed line has a slope of $-2.8$. (From Ref. 54.)

sufficiently long time scales, $t > \tau_1$, the relaxation time of the first normal mode (but $t < t_d$). In short time scales, $t < \tau_1$, the motion of the primitive chain is not a simple diffusion along its contour.

The test chain would follow the dynamics of the unrestricted Rouse chain if the entanglements were absent, as would the primitive chain at $t > t_e$. In Section 3.4.9, we considered the mean square displacement of monomers on the Rouse chain. We found that the dynamics is diffusional at $t < \tau_N$ and $\tau_1 < t$, where $\tau_N$ is the relaxation time of the $N$th normal mode but not in between. When the motion of the Rouse chain is restricted to the tube, the mean square displacement of monomers along the tube, $\langle [s(t) - s(0)]^2 \rangle$, will follow the same time dependence as the mean square displacement of the unrestricted Rouse chain in three dimensions. Thus, from Eqs. 3.240 and 3.243,

$$\langle [s(t) - s(0)]^2 \rangle \cong \begin{cases} Nb^2 (t/\tau_1)^{1/2} & (t_e < t < \tau_1) \\ D_c t & (\tau_1 < t) \end{cases} \tag{4.68}$$

where $D_c = k_B/N\zeta$ gives the center-of-mass diffusion coefficient of the Rouse chain in the absence of the entanglements.

We can map Eq. 4.68 onto the one-dimensional reptation dynamics, as we mapped a simple one-dimensional diffusion in Section 4.3.2.4. With Eq. 4.51 and $s = s(0)$ and $s' = s(t)$, we have

$$\langle [\mathbf{r}_n(t) - \mathbf{r}_n(0)]^2 \rangle \cong \begin{cases} N^{1/2} b b_t (t/\tau_1)^{1/4} & (t_e < t < \tau_1) \\ b_t (D_c t)^{1/2} & (\tau_1 < t < t_d) \end{cases} \tag{4.69}$$

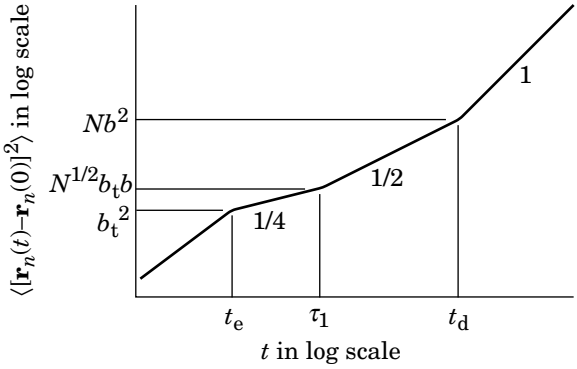


**Figure 4.43.** Mean square displacement of monomers on entangled chains, $\langle[\mathbf{r}_n(t) - \mathbf{r}_n(0)]^2\rangle$ plotted as a function of time $t$. The plot has four sections with distinct slopes. They are indicated adjacent to the plot. The boundaries of the four sections are specified by their values of $t$ and $\langle[\mathbf{r}_n(t) - \mathbf{r}_n(0)]^2\rangle$.

In the time scale of $t > t_d$, the effect of finding the new direction by the chain ends becomes dominant, and the mean square displacement of monomers will become equal to that of the center of mass. In the time scale of $t < t_e$, the motion of the monomers is complicated. At sufficiently short times ($t < \tau_N$), the monomers will make a diffusional motion without feeling the presence of other monomers, as we have seen for both the Rouse chain and the Zimm model. We can at least say that the dependence of $\langle[\mathbf{r}_n(t) - \mathbf{r}_n(0)]^2\rangle$ on $t$ is sharper at $t < t_e$.

Thus, we have the mean square displacement of monomers on the test chain for $t > t_e$ as

$$\langle[\mathbf{r}_n(t) - \mathbf{r}_n(0)]^2\rangle \cong \begin{cases} N^{1/2} b b_t (t/\tau_1)^{1/4} & (t_e < t < \tau_1) \\ b_t (D_c t)^{1/2} & (\tau_1 < t < t_d) \\ D_G t & (t_d < t) \end{cases} \quad \text{monomer diffusion by reptation} \tag{4.70}$$

Figure 4.43 illustrates the different regimes in the plot of $\langle[\mathbf{r}_n(t) - \mathbf{r}_n(0)]^2\rangle$. The boundary of each section is shown both for the time and the mean square displacement.

Presence of a section in which $\langle[\mathbf{r}_n(t) - \mathbf{r}_n(0)]^2\rangle \sim t^{1/2}$ is due to the reptation dynamics. Presence of a section in which $\langle[\mathbf{r}_n(t) - \mathbf{r}_n(0)]^2\rangle \sim t^{1/4}$ is due to the Rouse dynamics added on top of the reptation.

### 4.3.3 Problems

**Problem 4.11:** Estimate the tube diameter $b_t$ for solutions in the theta condition.

**Solution 4.11:** Comparison of Eqs. 4.60 and 4.64 with $m = -3$ leads to

$$b_t \cong (\zeta/\eta_s)^{1/2} b^{-4} \rho^{-3/2}$$